Journal of Computational Physics 228 (2009) 5763–5786

Contents lists available at ScienceDirect

Journal of Computational Physics

journal homepage: www.elsevier.com/locate/jcp

A finite volume method for approximating 3D diffusion operators on general meshes

F. Hermeline

CEA/DAM/DIF, Bruyères-le-Châtel, 91297 Arpajon Cedex, France

ARTICLE INFO

Article history:
Received 20 November 2008
Received in revised form 8 April 2009
Accepted 3 May 2009
Available online 9 May 2009

PACS:
65N30
76AA10
77A05

Keywords:
Elliptic equations
Anisotropic diffusion
Discrete duality finite volume method
Distorted meshes

ABSTRACT

A finite volume method is presented for discretizing 3D diffusion operators with variable full tensor coefficients. This method handles anisotropic, non-symmetric or discontinuous variable tensor coefficients while distorted, non-matching or non-convex *n*-faced polyhedron meshes can be used. For meshes of polyhedra whose faces have not more than four edges, the associated matrix is positive definite (and symmetric if the diffusion tensor is symmetric). A second-order (resp. first-order) accuracy is numerically observed for the solution (resp. gradient of the solution).

1. Introduction

The numerical modelling in many physics areas (for example: fluid flows in complex reservoir models, Lagrangian hydrodynamics with heat and radiative diffusion, Lagrangian magnetohydrodynamics with magnetic diffusion...) requires robust and flexible methods for approximating diffusion operators with variable full tensor coefficients on *arbitrary* (distorted, non-matching, non-convex...) unstructured *n*-sided (resp. *n*-faced) polygon (resp. polyhedron) meshes. For dealing with this problem, we proposed in [1,2] a new finite volume method, the principle of which is to integrate the equations both over a (given) *primal* mesh and an associated *dual* (or *covolume*) mesh that is made up from the primal mesh, the degrees of freedom being the values of the unknown function both at the mass centers and the vertices of the primal cells. In [3] this method has been generalized for handling *discontinuous* full tensor coefficients. Furthermore, in this same article, we proposed to use the so-called *indirect* dual mesh instead of the initial so-called *direct* dual mesh described in [2] (for definitions of these dual meshes see the next section). The indirect dual mesh lends itself better to the 3D framework and it provides a more accurate approximation of the gradient of the solution. Since then this type of method has been called *discrete duality finite volume* (DDFV) method in order to emphasize that it satisfies a discrete integration par parts (see [6]) and it proved to be efficient for dealing with several problems arising in various areas of computational physics (see [4–22]). Convergence analysis have been carried out in [5,12,18], for the linear case, and in [11] for the broad class of non-linear *Leray–Lions* type diffusion operators.

E-mail address: francois.hermeline@cea.fr

0021-9991/$ - see front matter © 2009 Elsevier Inc. All rights reserved.
doi:10.1016/j.jcp.2009.05.002

To our knowledge two 3D generalizations have been devised (while correcting this article we have been informed of an other type of 3D generalization: see [23]).

1. The first one, that leads generally to non-symmetric matrices, is proposed in [10]. This generalization is second-order accurate in the L^2 norm and it boils down to the usual cell-centered *and* vertex-centered finite volume methods when *Delaunay–Voronoi* meshes may be used. However the numerical experiments we have carried out since those displayed in [10] show that it is not robust enough to handle certain types of highly distorted meshes or highly anisotropic diffusion tensors.
2. The second one, that is more attractive because it provides symmetric positive definite matrices, is proposed in [8,19]. It has been used for approximating the so-called *bi-domain* equations that models the fully coupled heart and torso problem in electrocardiology.

Here we propose a third 3D generalization, inspired from the previous ones, that uses the indirect dual mesh instead of the dual mesh described in [8] which recovers *twice* the domain to be dealt with. The difference between this generalization and that proposed in [10] lies in the approximation of both the gradient operator and discontinuous tensor coefficients while the difference with that proposed in [8] lies in both the definition of the dual mesh and the approximation of discontinuous tensor coefficients. This third generalization provides symmetric positive definite matrices and is more robust than the first one. Furthermore it exhibits a numerical second-order accuracy in the L^2 norm for the solution and a first-order accuracy in the L^2 norm for the gradient of the solution (a nearly second-order accuracy in the L^2 norm for the gradient of the solution is even observed for the regular hexahedron meshes and for some distorted hexahedron meshes that have been tested below). However it is limited to polyhedral cells whose faces have *three* or *four* sides and it is not *monotone*. Such a 3D generalization with a theoretical study of the discrete duality property (which underlies the known convergence proofs of the 2D case) has been developed in [24].

Regarding other well-known methods for approximating diffusion operators in the framework of general meshes, one can quote the mixed hybrid finite element (MHFE), the multi-point-flux approximation (MPFA) or the mimetic finite difference (MFD) methods: the reader is referred, for example, to the (non-exhaustive) bibliography mentioned in [10]. Extensive 2D numerical comparisons between a lot of these methods have been carried out in [25] (see also the articles which follow this paper in the corresponding book). Other 2D numerical comparisons have been carried out in [26–29]. Recent works on 3D diffusion schemes may be found in [30–37].

The organization of the paper is as follows. Section 2 is devoted to the definition of the different meshes that will be used. The proposed finite volume method is set out in Section 3. Finally, several numerical experiments are presented in Section 4.

2. Meshes: definitions and notation

Before devising the proposed finite volume method some preliminary geometrical definitions are collected in this section.

Given Ω a polyhedral domain, we will use a mesh on Ω (called *primal* or *primary* mesh) made up of n-faced polyhedra. In what follows we define a "side" ("face") as being the one (two)-dimensional boundary shared by two polyhedra or by one polyhedron and the boundary of Ω. Note that such a side (face) may be not included in a straight line (plane). With each (primal) element P_p of this mesh we associate one (primal) point ξ_p: the mass center is a qualified candidate but other points could be chosen. By connecting these primal points, the barycenter ξ_f of every primal face F_f and the middle ξ_s of every primal side S_s we obtain a *dual* mesh on Ω (called *indirect*, *barycentric*, *median* or *Donald* dual mesh: see Fig. 1). With each (dual) element Π_d of this mesh we can associate one (dual) point $\mathbf{x}_d$, namely the point which belongs to the primal cells P_p whose associated primal point ξ_p is a vertex of Π_d. In all figures which follow the primal (resp. dual) points are denoted by the symbol $\circ$ (resp. $\bullet$) while the points ξ_f and ξ_s are denoted by the symbol $\square$. In addition of the indirect dual mesh, other available definitions of the dual mesh could be used such as the two following ones.

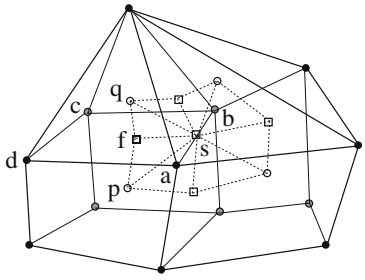

Fig. 1. *Full lines*: four primal cells (two hexahedra and two pyramids) sharing the side $S_s = \mathbf{x}_a\mathbf{x}_b$, two of them ($P_p$ and P_q) sharing the face $F_f = \mathbf{x}_a\mathbf{x}_b\mathbf{x}_c\mathbf{x}_d\xi_f$. *Dashed lines*: an indirect dual face shared by the dual cells Π_a and Π_b.

1. The first example is the so-called *direct* dual mesh obtained by connecting only the primal points ξ_p and the barycenters ξ_f of the *boundary* faces. However using such a dual mesh can be rather inconvenient because dual points may not belong to their associated dual cell, especially for highly distorted meshes. So the direct dual mesh will not be tested in what follows.
2. The second important example is the *Voronoi* mesh (see [38]). Assume that each primal polyhedron can be inscribed in a ball that does not contain any other vertex than those of this polyhedron (viz the primal mesh is a *Delaunay* mesh, see [39]). If all the ball centers are contained in Ω they can be chosen to be the primal interior points although some of them may not belong to their primal cell. By connecting these primal points and the centers of the boundary circumscribed circles, we obtain the so-called Voronoi dual mesh whose sides (faces) are perpendicular to the primal faces (sides). For more precisions regarding the numerical construction of such meshes see [40–44] and the bibliographies mentioned therein.

For the sake of clarity the definitions regarding the primal (resp. dual) mesh will be denoted by latin (resp. greek) letters. Given G a geometrical variable (side, face, polyhedron), we will denote by $|G|$ its measure (length, area or volume) and by ∂G its boundary.

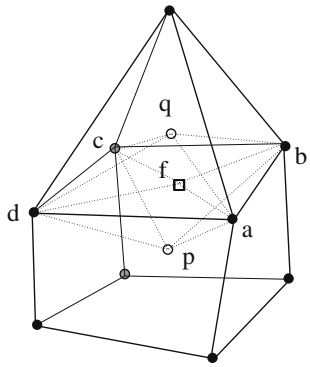

Fig. 2. *Full lines*: two primal cells (an hexahedron and a pyramid) sharing the face $F_f = \mathbf{x}_a\mathbf{x}_b\mathbf{x}_c\mathbf{x}_d\xi_f$. *Dotted lines*: the intermediary (diamond) cell $Q_f = \xi_p\mathbf{x}_a\mathbf{x}_b\mathbf{x}_c\mathbf{x}_d\xi_q$ associated with the primal face F_f.

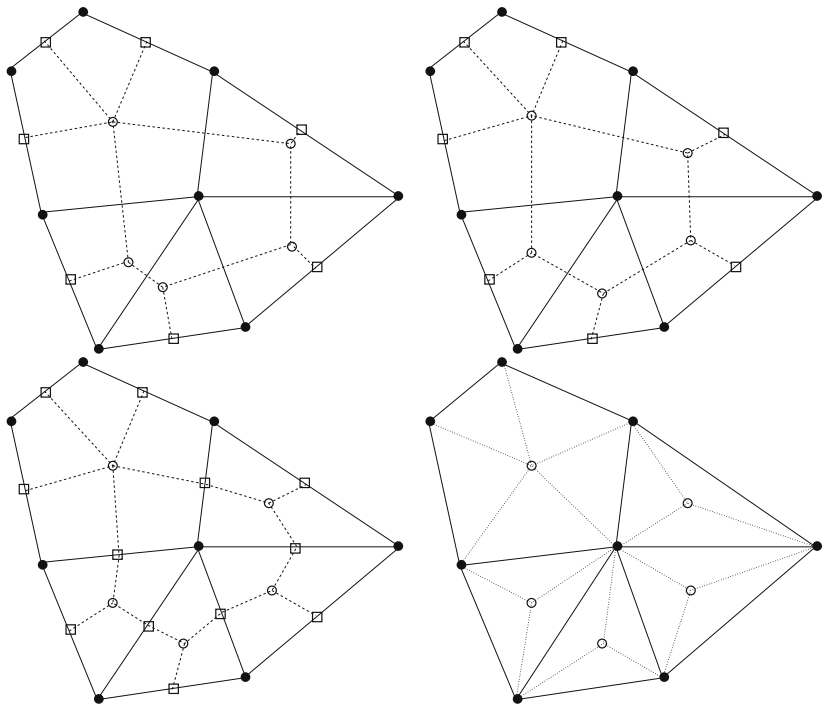

Fig. 3. A sample 2D primal mesh (full lines: four triangles and one pentagon) and its Voronoi dual mesh (dashed lines, top left), its direct dual mesh (dashed lines, top right), its indirect dual mesh (dashed lines, bottom left) and its intermediary (diamond) mesh (dotted lines, bottom right).

Besides the primal and dual meshes, we will need to define a third mesh: the so-called *intermediary* (or *diamond*) mesh. Suppose that each primal cell P_p is star-shaped with respect to its associated primal point ξ_p. For every face $F_f \in \partial P_p$ let be:

$$Q_{fp} = \bigcup_{\mathbf{x}\in F_f} [\mathbf{x}, \xi_p].$$

Suppose that F_f is an interior face such that $F_f = P_p \cap P_q$. By definition, the intermediary cell associated with F_f is $Q_f = Q_{fp} \cup Q_{fq}$. If F_f is a boundary face such that $F_f \in \partial P_p$ the intermediary cell associated with F_f is $Q_f = Q_{fp}$. By definition the set of intermediary cells is called the intermediary (or diamond) mesh of Ω (see Fig. 2).

Some 2D meshes illustrating these definitions are displayed on Fig. 3: note that corresponding 3D meshes are quite too complex to be drawn.

3. Discretization of the model elliptic equation

Given $\lambda = \lambda(\mathbf{x})$ a positive function, $\boldsymbol{\kappa} = \boldsymbol{\kappa}(\mathbf{x})$ a positive definite matrix, $f = f(\mathbf{x})$, $g = g(\mathbf{x})$ arbitrary functions and $\mathbf{n}$ the unit outward normal regarding the polyhedral domain Ω, we will focus on the approximation of the following model elliptic equation with a *Robin* (or *Fourier*) boundary condition:

$$\begin{cases} -\nabla \cdot (\boldsymbol{\kappa} \nabla u) = f & \text{in } \Omega, \\ \boldsymbol{\kappa} \nabla u \cdot \mathbf{n} + \lambda u = g & \text{on } \partial\Omega. \end{cases} \tag{1}$$

The principle of the proposed method lies in the following operations (Fig. 1):

- integrate the first equation over each primal polyhedron P_p,
- integrate the second equation through each *boundary* primal face F_f,
- integrate the first equation *multiplied by two* over each dual polyhedron Π_d,
- integrate the second equation through each *boundary* dual face $\partial\Pi_d \cap \partial\Omega$.

Thereby we obtain:

$$\begin{cases} -\int_{P_p} \nabla \cdot (\boldsymbol{\kappa} \nabla u) = \int_{P_p} f, \\ \int_{F_f} \boldsymbol{\kappa} \nabla u \cdot \mathbf{n} + \int_{F_f} \lambda u = \int_{F_f} g, \\ -2 \int_{\Pi_d} \nabla \cdot (\boldsymbol{\kappa} \nabla u) = 2 \int_{\Pi_d} f, \\ \int_{\partial\Pi_d \cap \partial\Omega} \boldsymbol{\kappa} \nabla u \cdot \mathbf{n} + \int_{\partial\Pi_d \cap \partial\Omega} \lambda u = \int_{\partial\Pi_d \cap \partial\Omega} g. \end{cases} \tag{2}$$

The multiplication by two does not seem natural. However we will see that it is necessary for obtaining a symmetric positive definite matrix: see [8] in which the author proposes to use a dual mesh that recovers twice the domain Ω.

In the light of (2) we have to provide approximations of both the divergence and gradient operators: this is the goal of the next two sections. The approximation of the other terms $\boldsymbol{\kappa}$, λ, f, g are described in Section 3.3. The degrees of freedom of the method will be the values of u at:

- the mass centers ξ_p of the primal cells P_p,
- the barycenters ξ_f of the boundary primal faces F_f,
- the vertices $\mathbf{x}_d$ of the primal cells P_p.

3.1. Divergence approximation

Let $\mathbf{v}$ be a vector function. Suppose that $\mathbf{v}_{fp}$ and $\mathbf{v}_{fq}$ are constant approximations of $\mathbf{v}$ in the intermediary sub-cells $Q_{fp} = Q_f \cap P_p$, $Q_{fq} = Q_f \cap P_q$. This section is aimed at providing an approximation of $\nabla \cdot \mathbf{v}$ that depends on the $\mathbf{v}_{fp}$, $\mathbf{v}_{fq}$ in both the primal and dual cells.

Let $\mathbf{n}$ ($\boldsymbol{\nu}$) be the unit outward normal vector regarding a primal (dual) cell. The divergence of $\mathbf{v}$ in the primal (dual) cell $P_p(\Pi_d)$ is approximated by:

$$(\nabla \cdot \mathbf{v})_p \simeq \frac{1}{|P_p|} \int_{P_p} \nabla \cdot \mathbf{v} = \frac{1}{|P_p|} \int_{\partial P_p} \mathbf{v} \cdot \mathbf{n},$$
$$(\nabla \cdot \mathbf{v})_d \simeq \frac{1}{|\Pi_d|} \int_{\Pi_d} \nabla \cdot \mathbf{v} = \frac{1}{|\Pi_d|} \int_{\partial\Pi_d} \mathbf{v} \cdot \boldsymbol{\nu}.$$

Let us denote (see Fig. 4):

$$F_f = \partial P_p \cap Q_f = \partial P_q \cap Q_f, \quad \Phi_{fd} = \partial\Pi_d \cap Q_f = \Phi_{frp} \cup \Phi_{fqr} \cup \Phi_{fup} \cup \Phi_{fqu},$$

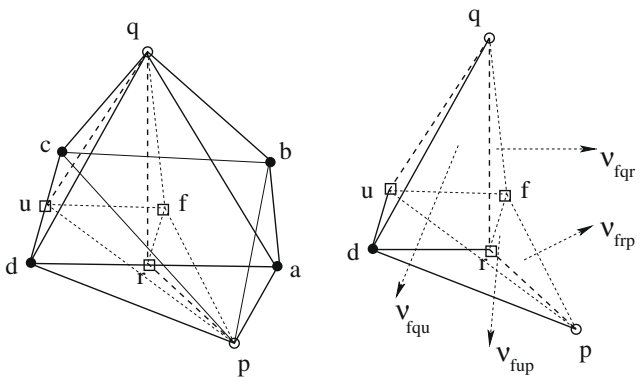

Fig. 4. *Left*: a quadrangular face $F_f = \mathbf{x}_a\mathbf{x}_b\mathbf{x}_c\mathbf{x}_d$ and its associated intermediary cell $Q_f = Q_{fp} \cup Q_{fq}$ with $Q_{fp} = \xi_p\mathbf{x}_a\mathbf{x}_b\mathbf{x}_c\mathbf{x}_d\xi_f$ et $Q_{fq} = \xi_q\mathbf{x}_a\mathbf{x}_b\mathbf{x}_c\mathbf{x}_d\xi_f$ (full lines). *Right*: dual sub-cell $\Pi_d \cap Q_f = \xi_p\mathbf{x}_d\xi_r\xi_f\ \xi_u\xi_q$ and its normals $\boldsymbol{\nu}_{frp}$, $\boldsymbol{\nu}_{fqr}$, $\boldsymbol{\nu}_{fup}$, $\boldsymbol{\nu}_{fqu}$.

where Φ_{frp}, Φ_{fqr}, Φ_{fup}, Φ_{fqu} are the triangular dual faces:

$$\Phi_{frp} = \xi_f\xi_r\xi_p, \quad \Phi_{fqr} = \xi_f\xi_q\xi_r, \quad \Phi_{fup} = \xi_f\xi_u\xi_p, \quad \Phi_{fqu} = \xi_f\xi_q\xi_u.$$

One remarks that:

$$\int_{\partial P_p} \mathbf{v}\cdot\mathbf{n} = \sum_{F_f\in\partial P_p} \int_{F_f} \mathbf{v}\cdot\mathbf{n}, \quad \int_{\partial \Pi_d} \mathbf{v}\cdot\boldsymbol{\nu} = \sum_{\Phi_{fd}\in\partial\Pi_d} \int_{\Phi_{fd}} \mathbf{v}\cdot\boldsymbol{\nu} + \int_{\partial\Pi_d\cap\partial\Omega} \mathbf{v}\cdot\mathbf{n}.$$

Let us denote:

$$\mathbf{n}_f = \int_{F_f} \mathbf{n},$$
$$\boldsymbol{\nu}_{frp} = \int_{\Phi_{frp}} \boldsymbol{\nu}, \quad \boldsymbol{\nu}_{fqr} = \int_{\Phi_{fqr}} \boldsymbol{\nu}, \quad \boldsymbol{\nu}_{fup} = \int_{\Phi_{fup}} \boldsymbol{\nu}, \quad \boldsymbol{\nu}_{fqu} = \int_{\Phi_{fqu}} \boldsymbol{\nu},$$

and (for $\mathbf{x}_d \in \partial\Omega$):

$$\mathbf{n}_d = \int_{\partial\Pi_d\cap\partial\Omega} \mathbf{n}.$$

We obtain the following approximations of $\nabla\cdot\mathbf{v}$ in P_p and Π_d:

$$\begin{cases} (\nabla\cdot\mathbf{v})_p = \frac{1}{|P_p|}\sum_{F_f\in\partial P_p} \mathbf{v}_{fp}\cdot\mathbf{n}_f, & (\xi_p \in \Omega), \\ (\nabla\cdot\mathbf{v})_d = \frac{1}{|\Pi_d|}\sum_{\Phi_{fd}\in\partial\Pi_d} \big(\mathbf{v}_{fp}\cdot(\boldsymbol{\nu}_{frp}-\boldsymbol{\nu}_{fup}) + \mathbf{v}_{fq}\cdot(\boldsymbol{\nu}_{fqr}-\boldsymbol{\nu}_{fqu})\big) & (\mathbf{x}_d \notin \partial\Omega), \\ (\nabla\cdot\mathbf{v})_d = \frac{1}{|\Pi_d|}\sum_{\Phi_{fd}\in\partial\Pi_d} \big(\mathbf{v}_{fp}\cdot(\boldsymbol{\nu}_{frp}-\boldsymbol{\nu}_{fup}) + \mathbf{v}_{fq}\cdot(\boldsymbol{\nu}_{fqr}-\boldsymbol{\nu}_{fqu})\big) + \frac{1}{|\Pi_d|}\mathbf{v}_d\cdot\mathbf{n}_d & (\mathbf{x}_d \in \partial\Omega). \end{cases} \tag{3}$$

For these approximations to be conservative, we have to set, for every interior intermediary cell $Q_f = Q_{fp} \cup Q_{fq}$:

$$\mathbf{v}_{fp}\cdot\mathbf{n}_f = \mathbf{v}_{fq}\cdot\mathbf{n}_f$$

(for example one can choose $\mathbf{v}_{fp} = \mathbf{v}_{fq} = \mathbf{v}_f$, where $\mathbf{v}_f$ is a piecewise constant approximation of $\mathbf{v}$ in Q_f).

3.2. Gradient approximation

Given a scalar function u, let u_p, u_f, u_d be the values of u at the points ξ_p, ξ_f, $\mathbf{x}_d$. The goal of this section is to provide approximations of ∇u that depends on the u_p, u_f, u_d.

3.2.1. Gradient approximation in the intermediary cells

Given a triangle $\mathbf{x}_a\mathbf{x}_b\mathbf{x}_c$, denote:

$$\mathbf{n}_{abc} = \frac{1}{2}(\mathbf{x}_b-\mathbf{x}_a)\times(\mathbf{x}_c-\mathbf{x}_a).$$

Suppose that u is linear in a tetrahedron T_{abcd}, we obtain the following value of ∇u in T_{abcd}:

$$(\nabla u)_{abcd} = \frac{1}{|T_{abcd}|}\int_{T_{abcd}} \nabla u = \frac{1}{|T_{abcd}|}\int_{\partial T_{abcd}} u\mathbf{n},$$

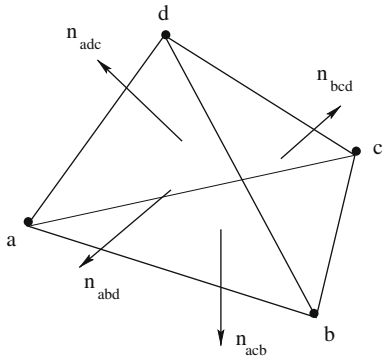

Fig. 5. A tetrahedron and its outward normals.

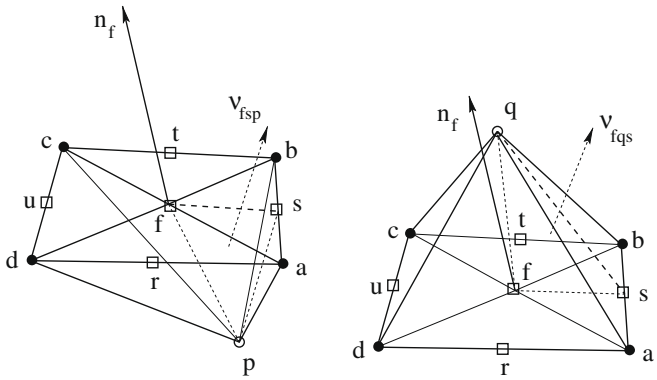

Fig. 6. *Left*: intermediary sub-cell $Q_{fp} = \xi_p \mathbf{x}_a\mathbf{x}_b\mathbf{x}_c\mathbf{x}_d\xi_f$ (full lines), primal face $F_f = \mathbf{x}_a\mathbf{x}_b\mathbf{x}_c\mathbf{x}_d$, dual sub-face $\Phi_{fsp} = \xi_f\xi_s\xi_p$ (dashed lines) and normals $\mathbf{n}_f$ and $\boldsymbol{\nu}_{fsp}$. *Right*: intermediary sub-cells $Q_{fq} = \xi_q\mathbf{x}_a\mathbf{x}_b\mathbf{x}_c\mathbf{x}_d\xi_f$ (full lines), primal face $F_f = \mathbf{x}_a\mathbf{x}_b\mathbf{x}_c\mathbf{x}_d$, dual sub-face $\Phi_{fqs} = \xi_f\xi_q\xi_s$ (dashed line) and normals $\mathbf{n}_f$ and $\boldsymbol{\nu}_{fqs}$.

that is (see Fig. 5):

$$(\nabla u)_{abcd} = \frac{1}{3}\frac{1}{|T_{abcd}|}((u_a + u_c + u_b)\mathbf{n}_{acb} + (u_a + u_b + u_d)\mathbf{n}_{abd} + (u_a + u_d + u_c)\mathbf{n}_{adc} + (u_b + u_c + u_d)\mathbf{n}_{bcd}).$$

By favouring the point $\mathbf{x}_a$, we obtain (because $\mathbf{n}_{acb} + \mathbf{n}_{adc} + \mathbf{n}_{abd} + \mathbf{n}_{bcd} = \mathbf{0}$):

$$(\nabla u)_{abcd} = \frac{1}{3}\frac{1}{|T_{abcd}|}((u_a - u_b)\mathbf{n}_{adc} + (u_a - u_c)\mathbf{n}_{abd} + (u_a - u_d)\mathbf{n}_{acb}). \tag{4}$$

For example, suppose that F_f is a quadrangular (but not necessary planar) face. Using formula (4) provides an approximation of ∇u in the eight tetrahedra T_{pdaf}, T_{pabf}, T_{pbcf}, T_{pcdf}, T_{qadf}, T_{qbaf}, T_{qcbf}, T_{qdcf} (see Fig. 6). The approximation $(\nabla u)_{fp}$ and $(\nabla u)_{fq}$ of ∇u in the intermediary sub-cells $Q_{fp} = T_{pdaf} \cup T_{pabf} \cup T_{pbcf} \cup T_{pcdf}$ and $Q_{fq} = T_{qadf} \cup T_{qbaf} \cup T_{qcbf} \cup T_{qdcf}$ is given by:

$$(\nabla u)_{fp} = \frac{|T_{pdaf}|(\nabla u)_{pdaf} + |T_{pabf}|(\nabla u)_{pabf} + |T_{pbcf}|(\nabla u)_{pbcf} + |T_{pcdf}|(\nabla u)_{pcdf}}{|T_{pdaf}| + |T_{pabf}| + |T_{pbcf}| + |T_{pcdf}|} \tag{5}$$

and:

$$(\nabla u)_{fq} = \frac{|T_{qadf}|(\nabla u)_{qadf} + |T_{qbaf}|(\nabla u)_{qbaf} + |T_{qcbf}|(\nabla u)_{qcbf} + |T_{qdcf}|(\nabla u)_{qdcf}}{|T_{qadf}| + |T_{qbaf}| + |T_{qcbf}| + |T_{qdcf}|}. \tag{6}$$

Let us denote:

$$\mathbf{n}_f = \int_{F_f} \mathbf{n}, \quad \boldsymbol{\nu}_{fsp} = \int_{\Phi_{fsp}} \boldsymbol{\nu}, \quad \boldsymbol{\nu}_{fqs} = \int_{\Phi_{fqs}} \boldsymbol{\nu}.$$

Replacing formula of type (4) in (5) and (6) provides:

$$\begin{cases} (\nabla u)_{fp} = \frac{1}{3}\frac{1}{|Q_{fp}|}\left((u_f - u_p)\mathbf{n}_f + 2\sum_{S_s\in\partial F_f}(u_b - u_a)\boldsymbol{v}_{fsp}\right), \\ (\nabla u)_{fq} = \frac{1}{3}\frac{1}{|Q_{fq}|}\left((u_q - u_f)\mathbf{n}_f + 2\sum_{S_s\in\partial F_f}(u_b - u_a)\boldsymbol{v}_{fqs}\right). \end{cases} \tag{7}$$

An approximation of ∇u in the *whole* intermediary cell Q_f is given by:

$$(\nabla u)_f = \frac{|Q_{fp}|(\nabla u)_{fp} + |Q_{fq}|(\nabla u)_{fq}}{|Q_{fp}| + |Q_{fq}|} = \frac{1}{3}\frac{1}{|Q_f|}\left((u_q - u_p)\mathbf{n}_f + 2\sum_{S_s\in\partial F_f}(u_b - u_a)\boldsymbol{v}_{fs}\right) \tag{8}$$

with $\boldsymbol{v}_{fs} = \boldsymbol{v}_{fsp} + \boldsymbol{v}_{fqs}$.

3.2.2. Gradient approximation in the primal and dual cells

If needed, an approximation of ∇u in the primal and dual cells can be given *from* the gradient approximation in the intermediary cells by setting:

$$(\nabla u)_p = \frac{1}{|P_p|}\sum_{F_f\in\partial P_p}|Q_{fp}|(\nabla u)_{fp}$$

and:

$$(\nabla u)_d = \frac{1}{|\Pi_d|}\sum_{\Sigma_f\in\partial\Pi_d}\left(|\Pi_d\cap Q_{fp}|(\nabla u)_{fp} + |\Pi_d\cap Q_{fq}|(\nabla u)_{fq}\right).$$

3.2.3. Remarks about the consistency

To give some idea of the consistency of the gradient approximation (8), let us consider a primal mesh made up of right parallelepipeds whose edge lengths are h_x, h_y, h_z and denote $\mathbf{e}_x = (1,0,0)$, $\mathbf{e}_y = (0,1,0)$, $\mathbf{e}_z = (0,0,1)$. In such a case we have:

$$|Q_f| = \frac{1}{3}h_x h_y h_z, \quad \mathbf{n}_f = h_x h_y \mathbf{e}_z, \quad \boldsymbol{v}_{fs} = -\boldsymbol{v}_{fu} = \frac{1}{4}h_x h_z \mathbf{e}_y, \quad \boldsymbol{v}_{fr} = -\boldsymbol{v}_{ft} = \frac{1}{4}h_y h_z \mathbf{e}_x$$

and the approximation (8) reads:

$$(\nabla u)_f = \frac{1}{2}\frac{1}{h_x h_y}(u_b - u_d)(h_y\mathbf{e}_x + h_x\mathbf{e}_y) + \frac{1}{2}\frac{1}{h_x h_y}(u_c - u_a)(-h_y\mathbf{e}_x + h_x\mathbf{e}_y) + \frac{1}{h_z}(u_q - u_p)\mathbf{e}_z. \tag{9}$$

Let denote by h_f the diameter of the intermediary cells Q_f. Given three arbitrary points $\mathbf{x}, \mathbf{y}, \mathbf{z} \in Q_f$, Taylor expansions provide:

$$u(\mathbf{y}) = u(\mathbf{x}) + (\mathbf{y} - \mathbf{x})\cdot\nabla u(\mathbf{x}) + o(h_f^2),$$
$$u(\mathbf{z}) = u(\mathbf{x}) + (\mathbf{z} - \mathbf{x})\cdot\nabla u(\mathbf{x}) + o(h_f^2),$$

whence:

$$u(\mathbf{y}) = u(\mathbf{z}) + (\mathbf{y} - \mathbf{z})\cdot\nabla u(\mathbf{x}) + o(h_f^2).$$

From this relation we deduce that there exists constants A, B, C such that:

$$u_b - u_d = (\mathbf{x}_b - \mathbf{x}_d)\cdot\nabla u(\mathbf{x}) + Ah_f^2,$$
$$u_c - u_a = (\mathbf{x}_c - \mathbf{x}_a)\cdot\nabla u(\mathbf{x}) + Bh_f^2,$$
$$u_q - u_p = (\xi_q - \xi_p)\cdot\nabla u(\mathbf{x}) + Ch_f^2,$$

that is (see Fig. 7):

$$u_b - u_d = (h_x\mathbf{e}_x + h_y\mathbf{e}_y)\cdot\nabla u(\mathbf{x}) + Ah_f^2,$$
$$u_c - u_a = (-h_x\mathbf{e}_x + h_y\mathbf{e}_y)\cdot\nabla u(\mathbf{x}) + Bh_f^2,$$
$$u_q - u_p = h_z\mathbf{e}_z\cdot\nabla u(\mathbf{x}) + Ch_f^2.$$

Replacing these values in (9) results in:

$$(\nabla u)_f = \nabla u(\mathbf{x}) + \mathbf{R}_f$$

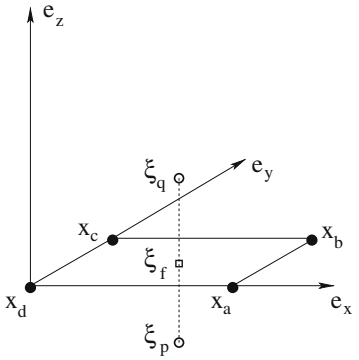

Fig. 7. *Right parallelepiped mesh*: a primal face $F_f = \mathbf{x}_a\mathbf{x}_b\mathbf{x}_c\mathbf{x}_d$ (full lines) and its associated dual side $\Sigma_f = \xi_p\xi_f\xi_q$ (dashed lines).

with:

$$\mathbf{R}_f = \left(\frac{1}{2}\frac{A}{h_x h_y}(h_y\mathbf{e}_x + h_x\mathbf{e}_y) + \frac{1}{2}\frac{B}{h_x h_y}(-h_y\mathbf{e}_x + h_x\mathbf{e}_y) + \frac{C}{h_z}\mathbf{e}_z\right)h_f^2.$$

It follows that:

$$|\mathbf{R}_f| \leqslant \max\left(\frac{1}{2}(A-B), \frac{1}{2}(A+B), C\right)\frac{h_f^2}{\min(h_x, h_y, h_z)}.$$

If there exists a positive value α such that:

$$\frac{h_f}{\min(h_x, h_y, h_z)} \leqslant \alpha$$

it follows that:

$$|(\nabla u)_f - \nabla u(\mathbf{x})| = o(h_f).$$

3.3. Approximation of the other terms

In the general case, one supposes that $\boldsymbol{\kappa}_{fp}$ and $\boldsymbol{\kappa}_{fq}$ are constant approximations of the diffusion coefficient $\boldsymbol{\kappa}$ in the intermediary sub-cell Q_{fp} and Q_{fq}, for example: $\boldsymbol{\kappa}_{fp} = \boldsymbol{\kappa}(\xi_p)$ and $\boldsymbol{\kappa}_{fq} = \boldsymbol{\kappa}(\xi_q)$. If $\boldsymbol{\kappa}$ is *continuous* in Q_f one replaces $\boldsymbol{\kappa}_{fp}$ and $\boldsymbol{\kappa}_{fq}$ by their arithmetic mean value or by the value $\boldsymbol{\kappa}(\xi_f)$.

For the other remaining terms, we set:

$$\int_{P_p} f = |P_p|f_p, \quad \int_{F_f} \lambda u = |F_f|\lambda_f u_f, \quad \int_{F_f} g = |F_f|g_f \tag{10}$$

and:

$$\int_{\Pi_d} f = |\Pi_d|f_d, \quad \int_{\partial\Pi_d\cap\partial\Omega} \lambda u = |\partial\Pi_d \cap \partial\Omega|\lambda_d u_d, \quad \int_{\partial\Pi_d\cap\partial\Omega} g = |\partial\Pi_d \cap \partial\Omega|g_d. \tag{11}$$

If f, λ, g have discontinuities that are honoured by the primal mesh, we will set:

$$\int_{\Pi_d} f = \sum_{P_p} |\Pi_d \cap P_p|f_p, \quad \int_{\partial\Pi_d\cap\partial\Omega} \lambda u = \sum_{F_f\in\partial\Omega} |\partial\Pi_d \cap F_f|\lambda_f u_d, \quad \int_{\partial\Pi_d\cap\partial\Omega} g = \sum_{F_f\in\partial\Omega} |\partial\Pi_d \cap F_f|g_f.$$

This amounts to replace f_d, λ_d, g_d in (11) by:

$$f_d = \frac{1}{|\Pi_d|}\sum_{P_p} |\Pi_d \cap P_p|f_p, \quad \lambda_d = \frac{1}{|\partial\Pi_d \cap \partial\Omega|}\sum_{F_f\in\partial\Omega} |\partial\Pi_d \cap F_f|\lambda_f, \quad g_d = \frac{1}{|\partial\Pi_d \cap \partial\Omega|}\sum_{F_f\in\partial\Omega} |\partial\Pi_d \cap F_f|g_f.$$

3.4. The linear system

Thanks to the approximations (3), (10) and (11) the system (2) reads:

$$\begin{cases} -\sum_{F_f\in\partial P_p} \mathbf{n}_f^t\cdot\boldsymbol{\kappa}_{fp}(\nabla u)_{fp} = |P_p|f_p & (\boldsymbol{\xi}_p\in\Omega),\\ \mathbf{n}_f^t\cdot\boldsymbol{\kappa}_{fp}(\nabla u)_{fp} + |F_f|\lambda_f u_f = |F_f|g_f & (\boldsymbol{\xi}_f\in\partial\Omega),\\ -2\sum_{\Phi_{fd}\in\partial\Pi_d}\left((\boldsymbol{v}_{frp}^t-\boldsymbol{v}_{fup}^t)\cdot\boldsymbol{\kappa}_{fp}(\nabla u)_{fp}+(\boldsymbol{v}_{fqr}^t-\boldsymbol{v}_{fqu}^t)\cdot\boldsymbol{\kappa}_{fq}(\nabla u)_{fq}\right) = 2|\Pi_d|f_d & (\mathbf{x}_d\notin\partial\Omega),\\ -2\sum_{\Phi_{fd}\in\partial\Pi_d}\left((\boldsymbol{v}_{frp}^t-\boldsymbol{v}_{fup}^t)\cdot\boldsymbol{\kappa}_{fp}(\nabla u)_{fp}+(\boldsymbol{v}_{fqr}^t-\boldsymbol{v}_{fqu}^t)\cdot\boldsymbol{\kappa}_{fq}(\nabla u)_{fq}\right) - 2\mathbf{n}_d^t\cdot\boldsymbol{\kappa}_d(\nabla u)_d = 2|\Pi_d|f_d & (\mathbf{x}_d\in\partial\Omega),\\ \mathbf{n}_d^t\cdot\boldsymbol{\kappa}_d(\nabla u)_d + |\partial\Pi_d\cap\partial\Omega|\lambda_d u_d = |\partial\Pi_d\cap\partial\Omega|g_d & (\mathbf{x}_d\in\partial\Omega). \end{cases} \tag{12}$$

Thanks to the approximations (7) we obtain:

$$\begin{cases} \mathbf{n}_f^t\cdot\boldsymbol{\kappa}_{fp}(\nabla u)_{fp} = \frac{1}{3}\frac{1}{|Q_{fp}|}\left(a_{fp}(u_f-u_p)+2\sum_{S_s\in\partial F_f} b_{fsp}(u_b-u_a)\right),\\ \mathbf{n}_f^t\cdot\boldsymbol{\kappa}_{fq}(\nabla u)_{fq} = \frac{1}{3}\frac{1}{|Q_{fq}|}\left(a_{fq}(u_q-u_f)+2\sum_{S_s\in\partial F_f} b_{fqs}(u_b-u_a)\right),\\ \boldsymbol{v}_{frp}^t\cdot\boldsymbol{\kappa}_{fp}(\nabla u)_{fp} = \frac{1}{3}\frac{1}{|Q_{fp}|}\left(\beta_{frp}(u_f-u_p)+2\sum_{S_s\in\partial F_f}\alpha_{frps}(u_b-u_a)\right),\\ \boldsymbol{v}_{fqr}^t\cdot\boldsymbol{\kappa}_{fq}(\nabla u)_{fq} = \frac{1}{3}\frac{1}{|Q_{fq}|}\left(\beta_{fqr}(u_q-u_f)+2\sum_{S_s\in\partial F_f}\alpha_{fqrs}(u_b-u_a)\right), \end{cases} \tag{13}$$

with:

$$\begin{cases} a_{fp}=\mathbf{n}_f^t\cdot\boldsymbol{\kappa}_{fp}\mathbf{n}_f, & a_{fq}=\mathbf{n}_f^t\cdot\boldsymbol{\kappa}_{fq}\mathbf{n}_f,\\ b_{fsp}=\mathbf{n}_f^t\cdot\boldsymbol{\kappa}_{fp}\boldsymbol{v}_{fsp}, & b_{fqs}=\mathbf{n}_f^t\cdot\boldsymbol{\kappa}_{fq}\boldsymbol{v}_{fqs},\\ \alpha_{frps}=\boldsymbol{v}_{frp}^t\cdot\boldsymbol{\kappa}_{fp}\boldsymbol{v}_{fsp}, & a_{fqrs}=\boldsymbol{v}_{fqr}^t\cdot\boldsymbol{\kappa}_{fq}\boldsymbol{v}_{fqs},\\ \beta_{frp}=\boldsymbol{v}_{frp}^t\cdot\boldsymbol{\kappa}_{fp}\mathbf{n}_f, & \beta_{fqr}=\boldsymbol{v}_{fqr}^t\cdot\boldsymbol{\kappa}_{fq}\mathbf{n}_f. \end{cases}$$

The *interior* values u_f are eliminated by using the equality of normal fluxes:

$$\mathbf{n}_f^t\cdot\boldsymbol{\kappa}_{fp}(\nabla u)_{fp} = \mathbf{n}_f^t\cdot\boldsymbol{\kappa}_{fq}(\nabla u)_{fq}. \tag{14}$$

Thus we obtain:

$$u_f = \frac{1}{a_{fp}|Q_{fq}|+a_{fq}|Q_{fp}|}\left(a_{fp}|Q_{fq}|u_p + a_{fq}|Q_{fp}|u_q - 2\sum_{S_s\in\partial F_f}(b_{fsp}|Q_{fq}|-b_{fqs}|Q_{fp}|)(u_b-u_a)\right).$$

Both replacing (13) in (12) and eliminating the boundary degrees of freedom $\mathbf{n}_d^t\cdot\boldsymbol{\kappa}_d(\nabla u)_d$ results in the following linear system of N equations in N unknowns u_p, $u_f(F_f\in\partial\Omega)$, u_d(N = number of primal cells + number of boundary primal faces + number of vertices of the primal mesh):

$$\begin{cases} \sum_{F_f\in\partial P_p} A_f(u_p-u_q) + \sum_{F_f\in\partial P_p}\sum_{S_s\in\partial F_f} B_{fs}(u_a-u_b) = |P_p|f_p & (\boldsymbol{\xi}_p\in\Omega),\\ A_f(u_f-u_p) - \sum_{S_s\in\partial F_f} B_{fs}(u_a-u_b) + |F_f|\lambda_f u_f = |F_f|g_f & (\boldsymbol{\xi}_f\in\partial\Omega),\\ \sum_{\Phi_{fd}\in\partial\Pi_d} C_{fd}(u_p-u_q) + \sum_{\Phi_{fd}\in\partial\Pi_d}\sum_{S_s\in\partial F_f} D_{fds}(u_a-u_b)d = 2|\Pi_d|f_d & (\mathbf{x}_d\notin\Omega),\\ \sum_{\Phi_{fd}\in\partial\Pi_d} C_{fd}(u_p-u_q) + \sum_{\Phi_{fd}\in\partial\Pi_d}\sum_{S_s\in\partial F_f} D_{fds}(u_a-u_b) + 2|\partial\Pi_d\cap\partial\Omega|\lambda_d u_d = 2|\Pi_d|f_d + 2|\partial\Pi_d\cap\partial\Omega|g_d & (\mathbf{x}_d\in\Omega), \end{cases} \tag{15}$$

with:

$$\begin{cases} A_f = \frac{1}{3}\frac{a_{fp}a_{fq}}{a_{fp}|Q_{fq}|+a_{fq}|Q_{fp}|},\\ B_{fs} = \frac{2}{3}\frac{a_{fp}b_{fqs}+a_{fq}b_{fsp}}{a_{fp}|Q_{fq}|+a_{fq}|Q_{fp}|},\\ C_{fd} = \frac{2}{3}\frac{a_{fp}(\beta_{fqr}-\beta_{fqu})+a_{fq}(\beta_{frp}-\beta_{fup})}{a_{fp}|Q_{fq}|+a_{fq}|Q_{fp}|},\\ D_{fds} = \frac{4}{3}\frac{(\alpha_{frps}-\alpha_{fups})|Q_{fq}|+(\alpha_{fqrs}-\alpha_{fqus})|Q_{fp}|}{|Q_{fp}||Q_{fq}|} - \frac{4}{3}\frac{\left(b_{fsp}|Q_{fq}|-b_{fqs}|Q_{fp}|\right)\left((\beta_{frp}-\beta_{fup})|Q_{fq}|-(\beta_{fqr}-\beta_{fqu})|Q_{fp}|\right)}{|Q_{fp}||Q_{fq}|(a_{fp}|Q_{fq}|+a_{fq}|Q_{fp}|)}. \end{cases}$$

If Q_f is a *boundary* intermediary cell, note that:

$$A_f = \frac{1}{3}\frac{a_{fp}}{|Q_{fp}|}, \quad B_{fs} = \frac{2}{3}\frac{b_{fsp}}{|Q_{fp}|}, \quad C_{fd} = \frac{2}{3}\frac{\beta_{frp} - \beta_{fup}}{|Q_{fp}|}, \quad D_{fds} = \frac{4}{3}\frac{\alpha_{frps} - \alpha_{fups}}{|Q_{fp}|}.$$

3.5. Properties of the linear system

Let $\mathbf{u}$ be the column-vector made up of the unknowns u_p, $u_f(\xi_f \in \partial\Omega)$, u_d and let $\mathbf{f}$ be the column-vector made up of values $|P_p|f_p$,$|F_f|g_f(\xi_f \in \partial\Omega)$, $|\Pi_d|f_d + |\Pi_d \cap \partial\Omega|g_d$. The linear system (15) can be rewritten as:

$$\mathbf{Ku} = \mathbf{f}.$$

Note that $\mathbf{K}$ is not an M-matrix (because non-diagonal coefficients may be strictly positive), so we cannot hope that $\mathbf{K}$ be monotone in general. On the other hand one can prove the following theorem.

Theorem 1. *The matrix* $\mathbf{K}$ *is positive and it is symmetric if* κ *is symmetric. If every face of the primal cells has three or four sides it is also definite.*

Proof. Let w be a test function. We have:

$$\frac{1}{3}\mathbf{w}^t \cdot \mathbf{Ku} = I(\mathbf{u},\mathbf{w}) + B(\mathbf{u},\mathbf{w}) = S(\mathbf{w}),$$

where I, B ,S are what we can call respectively an interior energy term:

$$\begin{cases} I(\mathbf{u},\mathbf{w}) = -\frac{1}{3}\sum\limits_{P_p}\sum\limits_{F_f\in\partial P_p} \mathbf{n}_f^t \cdot \boldsymbol{\kappa}_{fp}(\nabla u)_{fp} w_p + \frac{1}{3}\sum\limits_{F_f\in\partial\Omega} \mathbf{n}_f^t \cdot \boldsymbol{\kappa}_{fp}(\nabla u)_{fp} w_f \\ \qquad -\frac{2}{3}\sum\limits_{\Pi_d}\sum\limits_{\Phi_{fd}\in\partial\Pi_d} \Big((\boldsymbol{v}_{frp}^t - \boldsymbol{v}_{fup}^t)\cdot\boldsymbol{\kappa}_{fp}(\nabla u)_{fp} + (\boldsymbol{v}_{fqr}^t - \boldsymbol{v}_{fqu}^t)\cdot\boldsymbol{\kappa}_{fq}(\nabla u)_{fq}\Big) w_d, \end{cases}$$

a boundary energy term:

$$B(\mathbf{u},\mathbf{w}) = \frac{1}{3}\sum_{F_f\in\partial\Omega} |F_f|\lambda_f u_f w_f + \frac{2}{3}\sum_{\mathbf{x}_d\in\partial\Omega} |\partial\Pi_d \cap \partial\Omega|\lambda_d u_d w_d$$

and a source term:

$$S(\mathbf{w}) = \frac{1}{3}\sum_{P_p} |P_p|f_p w_p + \frac{2}{3}\sum_{\Pi_d} |\Pi_d|f_d w_d + \frac{1}{3}\sum_{F_f\in\partial\Omega} |F_f|g_f w_f + \frac{2}{3}\sum_{\mathbf{x}_d\in\partial\Omega} |\partial\Pi_d \cap \partial\Omega|g_d w_d.$$

The term $I(\mathbf{u},\mathbf{w})$ can be rewritten as:

$$\begin{cases} I(\mathbf{u},\mathbf{w}) = \frac{1}{3}\sum\limits_{F_f\notin\partial\Omega}\Big(-\mathbf{n}_f^t \cdot \boldsymbol{\kappa}_{fp}(\nabla u)_{fp} w_p + \mathbf{n}_f^t \cdot \boldsymbol{\kappa}_{fq}(\nabla u)_{fq} w_q\Big) \\ \qquad -\frac{2}{3}\sum\limits_{F_f\notin\partial\Omega}\sum\limits_{\mathbf{x}_d\in\partial F_f} \Big((\boldsymbol{v}_{frp}^t - \boldsymbol{v}_{fup}^t)\cdot\boldsymbol{\kappa}_{fp}(\nabla u)_{fp} + (\boldsymbol{v}_{fqr}^t - \boldsymbol{v}_{fqu}^t)\cdot\boldsymbol{\kappa}_{fq}(\nabla u)_{fq}\Big) w_d \\ \qquad +\frac{1}{3}\sum\limits_{F_f\in\partial\Omega} \mathbf{n}_f^t \cdot \boldsymbol{\kappa}_{fp}(\nabla u)_{fp} w_f - \frac{1}{3}\sum\limits_{F_f\in\partial\Omega} \mathbf{n}_f^t \cdot \boldsymbol{\kappa}_{fp}(\nabla u)_{fp} w_p \\ \qquad -\frac{2}{3}\sum\limits_{F_f\in\partial\Omega}\sum\limits_{\mathbf{x}_d\in\partial F_f} (\boldsymbol{v}_{frp}^t - \boldsymbol{v}_{fup}^t)\cdot\boldsymbol{\kappa}_{fp}(\nabla u)_{fp} w_d. \end{cases}$$

Let us introduce the values w_f of the test function w at the interior points ξ_f. Thanks to the equality of the normal fluxes (14) we obtain:

$$\begin{cases} I(\mathbf{u},\mathbf{w}) = \frac{1}{3}\sum\limits_{F_f}\left(\mathbf{n}_f^t \cdot \boldsymbol{\kappa}_{fp}(\nabla u)_{fp}(w_f - w_p) - 2\sum\limits_{\mathbf{x}_d\in\partial F_f} (\boldsymbol{v}_{frp}^t - \boldsymbol{v}_{fup}^t)\cdot\boldsymbol{\kappa}_{fp}(\nabla u)_{fp} w_d\right) \\ \qquad +\frac{1}{3}\sum\limits_{F_f\notin\partial\Omega}\left(\mathbf{n}_f^t \cdot \boldsymbol{\kappa}_{fq}(\nabla u)_{fq}(w_q - w_f) - 2\sum\limits_{\mathbf{x}_d\in\partial F_f} (\boldsymbol{v}_{fqr}^t - \boldsymbol{v}_{fqu}^t)\cdot\boldsymbol{\kappa}_{fq}(\nabla u)_{fq} w_d\right). \end{cases}$$

Thanks to the identities:

$$\sum_{\mathbf{x}_d\in\partial F_f} (\boldsymbol{v}_{frp}^t - \boldsymbol{v}_{fup}^t)\cdot\boldsymbol{\kappa}_{fp}(\nabla u)_{fp} w_d = -\sum_{S_s\in\partial F_f} \boldsymbol{v}_{fsp}^t \cdot \boldsymbol{\kappa}_{fp}(\nabla u)_{fp}(w_b - w_a),$$
$$\sum_{\mathbf{x}_d\in\partial F_f} (\boldsymbol{v}_{fqr}^t - \boldsymbol{v}_{fqu}^t)\cdot\boldsymbol{\kappa}_{fq}(\nabla u)_{fq} w_d = -\sum_{S_s\in\partial F_f} \boldsymbol{v}_{fqs}^t \cdot \boldsymbol{\kappa}_{fq}(\nabla u)_{fq}(w_b - w_a),$$

and thanks to the definition of $(\nabla w)_{fp}, (\nabla w)_{fq}$:

$$(\nabla w)_{fp} = \frac{1}{3}\frac{1}{|Q_{fp}|}\left((w_f - w_p)\mathbf{n}_f + 2\sum_{S_s\in\partial F_f}(w_b - w_a)\boldsymbol{v}_{fsp}\right),$$
$$(\nabla w)_{fq} = \frac{1}{3}\frac{1}{|Q_{fq}|}\left((w_q - w_f)\mathbf{n}_f + 2\sum_{S_s\in\partial F_f}(w_b - w_a)\boldsymbol{v}_{fqs}\right),$$

we obtain finally the following identity:

$$\begin{cases} I(\mathbf{u},\mathbf{w}) = -\frac{1}{3}\sum_{P_p}\sum_{F_f\in\partial P_p}\mathbf{n}_f^t\cdot\boldsymbol{\kappa}_{fp}(\nabla u)_{fp}w_p + \frac{1}{3}\sum_{F_f\in\partial\Omega}\mathbf{n}_f^t\cdot\boldsymbol{\kappa}_{fp}(\nabla u)_{fp}w_f \\ \qquad -\frac{2}{3}\sum_{\Pi_d}\sum_{\Phi_{fd}\in\partial\Pi_d}\left((\boldsymbol{v}_{frp}^t - \boldsymbol{v}_{fup}^t)\cdot\boldsymbol{\kappa}_{fp}(\nabla u)_{fp} + (\boldsymbol{v}_{fqr}^t - \boldsymbol{v}_{fqu}^t)\cdot\boldsymbol{\kappa}_{fq}(\nabla u)_{fq}\right)w_d \\ \qquad = \sum_{F_f}|Q_{fp}|(\nabla w)_{fp}^t\cdot\boldsymbol{\kappa}_{fp}(\nabla u)_{fp} + \sum_{F_f\notin\partial\Omega}|Q_{fq}|(\nabla w)_{fq}^t\cdot\boldsymbol{\kappa}_{fq}(\nabla u)_{fq} \end{cases}$$

which is a discrete equivalent of the integration par parts:

$$-\int_\Omega \nabla\cdot(\boldsymbol{\kappa}\nabla u)w + \int_{\partial\Omega}\mathbf{n}^t\cdot\boldsymbol{\kappa}\nabla u w = \int_\Omega(\boldsymbol{\kappa}\nabla u)\cdot\nabla w.$$

In [6] this type of relation has been called "discrete duality", thus giving its name to the class of the discrete duality finite volume (DDFV) methods. From this relation we deduce that the matrix associated with (15) is positive (because $I(\mathbf{u},\mathbf{u}) + B(\mathbf{u},\mathbf{u}) \geqslant 0$) and symmetric (provided that κ_{fp} and κ_{fq} are symmetric).

If $f = 0$ and $g = 0$ we obtain: $I(\mathbf{u},\mathbf{u}) + B(\mathbf{u},\mathbf{u}) = S(\mathbf{u}) = 0$ therefore $(\nabla u)_{fp} = (\nabla u)_{fq} = \mathbf{0}$ (for all f) and $u_f = u_d = 0$ (for all ξ_f, $\mathbf{x}_d \in \partial\Omega$). For any face F_f, the vectors v_{fsp} ($S_s \in \partial F_f$) in the one hand and v_{fqs} ($S_s \in \partial F_f$) in the other hand, are all included in a plane that does not contain $\mathbf{n}_f$. From the definition (7) of $(\nabla u)_{fp}$ and $(\nabla u)_{fq}$, it follows that:

$$(u_f - u_p)\mathbf{n}_f = (u_q - u_f)\mathbf{n}_f = \mathbf{0}, \tag{16}$$

and:

$$\sum_{S_s\in\partial F_f}(u_b - u_a)\boldsymbol{v}_{fsp} = \sum_{S_s\in\partial F_f}(u_b - u_a)\boldsymbol{v}_{fqs} = \mathbf{0}. \tag{17}$$

From (16) it follows that $u_f = u_p = u_q$. If there exists a point $\xi_f \in \partial\Omega$ such that $\lambda_f \neq 0$ then all the degrees of freedom u_p, $u_f(\xi_f \in \partial\Omega)$ are zero.

Arrived at this point it remains to prove that $u_d = 0$ for all $\mathbf{x}_d$. One can distinguish three cases.

1. If the primal face F_f is triangular ($F_f = \mathbf{x}_a\mathbf{x}_b\mathbf{x}_c$, see Fig. 8), the relation (17) reads:

   $$(u_b - u_a)\boldsymbol{v}_{fsp} + (u_c - u_b)\boldsymbol{v}_{ftp} + (u_a - u_c)\boldsymbol{v}_{frp} = \mathbf{0},$$

   that is, for example:

   $$(u_b - u_a)(\boldsymbol{v}_{fsp} - \boldsymbol{v}_{frp}) + (u_c - u_b)(\boldsymbol{v}_{ftp} - \boldsymbol{v}_{frp}) = \mathbf{0}.$$

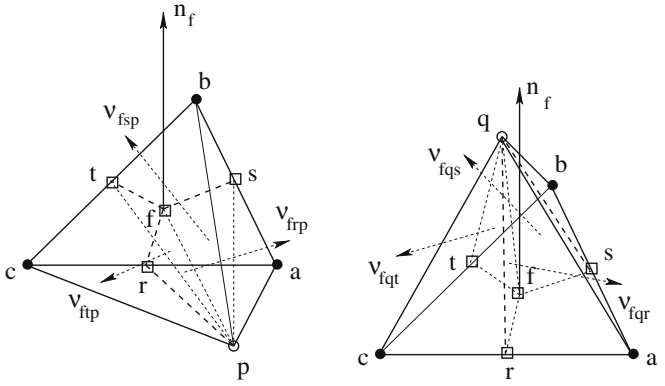

Fig. 8. *Left*: intermediary sub-cell $Q_{fp} = \xi_p\mathbf{x}_a\mathbf{x}_b\mathbf{x}_c\xi_f$ (full lines), primal face $F_f = \mathbf{x}_a\mathbf{x}_b\mathbf{x}_c$, dual sub-faces $\Phi_{fsp} = \xi_f\xi_s\xi_p$, $\Phi_{ftp} = \xi_f\xi_t\xi_p$, $\Phi_{frp} = \xi_f\xi_r\xi_p$ (dashed lines) and normals $\mathbf{n}_f$ and $\boldsymbol{v}_{frp}$, $\boldsymbol{v}_{fsp}$, $\boldsymbol{v}_{ftp}$. *Right*: intermediary sub-cells $Q_{fq} = \xi_q\mathbf{x}_a\mathbf{x}_b\mathbf{x}_c\xi_f$ (full lines), primal face $F_f = \mathbf{x}_a\mathbf{x}_b\mathbf{x}_c$, dual sub-faces $\Phi_{fqs} = \xi_f\xi_q\xi_s$, $\Phi_{fqt} = \xi_f\xi_q\ \xi_t$, $\Phi_{fqs} = \xi_f\xi_q\xi_r$ (dashed line) and normals $\mathbf{n}_f$ and $\boldsymbol{v}_{fqr}$, $\boldsymbol{v}_{fqs}$, $\boldsymbol{v}_{fqt}$.

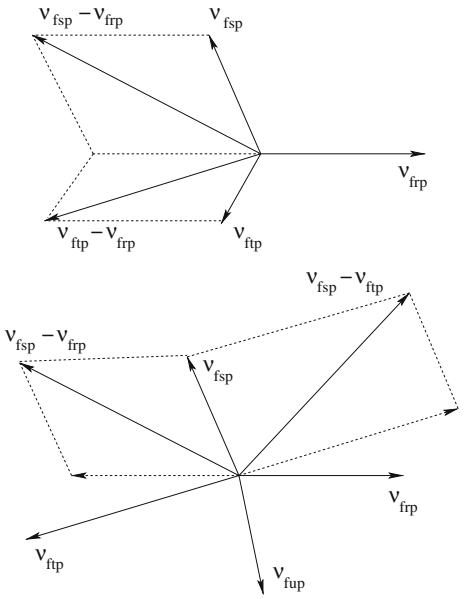

Fig. 9. *Top*: vectors $\boldsymbol{v}_{frp}$, $\boldsymbol{v}_{fsp}$, $\boldsymbol{v}_{ftp}$ in the plane perpendicular to $\xi_p\xi_f$ (for a triangular face F_f). *Bottom*: vectors $\boldsymbol{v}_{frp}$, $\boldsymbol{v}_{fsp}$, $\boldsymbol{v}_{ftp}$, $\boldsymbol{v}_{fup}$ in the plane perpendicular to $\xi_p\xi_f$ (for a quadrangular face F_f).

Since the vectors $v_{fsp} - v_{frp}$ and $v_{ftp} - v_{frp}$ are linearly independent (see Fig. 9 top), we obtain: $u_a = u_b = u_c$. If the primal mesh is made up of tetrahedra and if there exists a point $\mathbf{x}_d \in \partial\Omega$ such that $\lambda_d \neq 0$, then all the degrees of freedom u_d are zero.

2. If the primal face F_f is quadrangular ($F_f = \mathbf{x}_a\mathbf{x}_b\mathbf{x}_c\mathbf{x}_d$, see Fig. 6), the relation (17) reads:

$$(u_b - u_a)\boldsymbol{v}_{fsp} + (u_c - u_b)\boldsymbol{v}_{ftp} + (u_d - u_c)\boldsymbol{v}_{fup} + (u_a - u_d)\boldsymbol{v}_{frp} = \mathbf{0}$$

that is:

$$u_a(\boldsymbol{v}_{frp} - \boldsymbol{v}_{fsp}) + u_b(\boldsymbol{v}_{fsp} - \boldsymbol{v}_{ftp}) + u_c(\boldsymbol{v}_{ftp} - \boldsymbol{v}_{fup}) + u_d(\boldsymbol{v}_{fup} - \boldsymbol{v}_{frp}) = \mathbf{0}. \tag{18}$$

Since $\xi_r(\xi_s, \xi_t, \xi_u)$ are the middle of the sides $S_r(S_s, S_t, S_u)$ of the primal face F_f, elementary geometrical considerations give:

$$\begin{aligned}
&-\boldsymbol{v}_{fsp} + \boldsymbol{v}_{ftp} + \frac{1}{2}(\mathbf{n}_{fab} + \mathbf{n}_{fbc}) + \frac{1}{2}(\boldsymbol{v}_{pba} + \boldsymbol{v}_{pcb}) = \mathbf{0},\\
&-\boldsymbol{v}_{ftp} + \boldsymbol{v}_{fup} + \frac{1}{2}(\mathbf{n}_{fbc} + \mathbf{n}_{fcd}) + \frac{1}{2}(\boldsymbol{v}_{pcb} + \boldsymbol{v}_{pdc}) = \mathbf{0},\\
&-\boldsymbol{v}_{fup} + \boldsymbol{v}_{frp} + \frac{1}{2}(\mathbf{n}_{fcd} + \mathbf{n}_{fda}) + \frac{1}{2}(\boldsymbol{v}_{pdc} + \boldsymbol{v}_{pad}) = \mathbf{0},\\
&-\boldsymbol{v}_{frp} + \boldsymbol{v}_{fsp} + \frac{1}{2}(\mathbf{n}_{fda} + \mathbf{n}_{fab}) + \frac{1}{2}(\boldsymbol{v}_{pad} + \boldsymbol{v}_{pba}) = \mathbf{0}.
\end{aligned}$$

Adding the first and third (or second and fourth) equations and noting that:

$$\mathbf{n}_{fab} + \mathbf{n}_{fbc} + \mathbf{n}_{fcd} + \mathbf{n}_{fda} + \boldsymbol{v}_{pba} + \boldsymbol{v}_{pcb} + \boldsymbol{v}_{pdc} + \boldsymbol{v}_{pad} = \mathbf{0},$$

provides:

$$-\boldsymbol{v}_{fsp} + \boldsymbol{v}_{ftp} - \boldsymbol{v}_{fup} + \boldsymbol{v}_{frp} = \mathbf{0}.$$

By taking into account this relation, (18) reads:

$$(u_c - u_a)(\boldsymbol{v}_{fsp} - \boldsymbol{v}_{frp}) + (u_b - u_d)(\boldsymbol{v}_{fsp} - \boldsymbol{v}_{ftp}) = \mathbf{0}.$$

Since the vectors $v_{frp} - v_{fsp}$ and $v_{fsp} - v_{ftp}$ are linearly independent (see Fig. 9 bottom), we obtain: $u_a = u_c$ and $u_b = u_d$. If the primal mesh is made up of hexahedra (or mixed tetrahedra and hexahedra) and if there exists *two* points $\mathbf{x}_c$, $\mathbf{x}_d \in \partial\Omega$ that are the vertices of one side of a boundary quadrangular primal face, such that $\lambda_c \neq 0$, $\lambda_d \neq 0$, then all the degrees of freedom u_d are zero.

3. If the primal face F_f has more than four sides we cannot conclude: the matrix $\mathbf{K}$ is only positive semidefinite.

This ends the proof. It is worth remarking that the matrix $\mathbf{K}$ coincides with the matrix associated with the method proposed in [8] (although the dual meshes are different) as soon as:

1. the indirect dual mesh is replaced by the direct dual mesh,
2. discontinuous tensors κ are not involved.

3.6. Dealing with the Dirichlet boundary condition

In order to keep the presentation simpler, the Dirichlet or mixed Dirichlet–Robin boundary conditions have not been considered so far. Assume that $\partial\Omega = \overline{\Gamma}_R \cup \overline{\Gamma}_D$ (where Γ_R, Γ_D are disjoint open subsets of $\partial\Omega$) and that:

$$\begin{cases} \boldsymbol{\kappa}\nabla u \cdot \mathbf{n} + \lambda u = g & \text{on} \quad \Gamma_R, \\ u = v & \text{on} \quad \overline{\Gamma}_D. \end{cases}$$

The Dirichlet boundary condition: $u = v$ on $\overline{\Gamma}_D$ may be numerically embodied in the Robin boundary condition, provided that $g = \lambda v$ on $\overline{\Gamma}_D$ and that λ is chosen large enough. An other way (that we have chosen) consists in imposing $u_f = v_f$ and $u_d = v_d$ for all $\xi_f, \mathbf{x}_d \in \overline{\Gamma}_d$ when iterative methods are used for solving the linear system (15).

Note that we will suppose that the primal mesh honours the boundary $\overline{\Gamma}_R \cap \overline{\Gamma}_D$ when mixed Dirichlet–Robin boundary conditions have to be handled.

3.7. Particular cases

Let us define (see Fig. 8 for example):

1. θ_{fp} (θ_{fq}) the angle between $\mathbf{n}_f$ and the dual side $\Sigma_{fp} = \xi_f\xi_p$ ($\Sigma_{fq} = \xi_f\xi_q$),
2. η_{frps} (η_{fqrs}) the angle between $\boldsymbol{\nu}_{frp}$ and $\boldsymbol{\nu}_{fsp}$ ($\boldsymbol{\nu}_{fqr}$ and $\boldsymbol{\nu}_{fqs}$),
3. ζ_{fsp} (ζ_{fqs}) the angle between $\mathbf{n}_f$ and $\boldsymbol{\nu}_{fsp}$ ($\boldsymbol{\nu}_{fqs}$).

Suppose that F_f is a planar face and $\xi_f \in F_f$. The volume of the intermediary sub-cells Q_{fp} and Q_{fq} are given by:

$$|Q_{fp}| = \frac{1}{3} h_{fp} |F_f|, \quad |Q_{fq}| = \frac{1}{3} h_{fq} |F_f|,$$

where:

$$h_{fp} = \cos\theta_{fp} |\Sigma_{fp}|, \quad h_{fq} = \cos\theta_{fq} |\Sigma_{fq}|$$

are the distances between the point ξ_p (ξ_q) and the face F_f.

Furthermore suppose that the diffusion coefficient $\boldsymbol{\kappa}$ is continuous and isotropic (that is $\boldsymbol{\kappa} = \kappa\mathbf{I}$, κ being a strictly positive continuous function) and denote:

$$\kappa_f = \frac{1}{2}(\kappa_{fp} + \kappa_{fq}),$$

we obtain:

$$a_{fp} = a_{fq} = \kappa_f |F_f|^2, \quad \alpha_{frps} = \kappa_f \cos\eta_{frps} |\Phi_{frp}||\Phi_{fsp}|, \quad \alpha_{fqrs} = \kappa_f \cos\eta_{fqrs} |\Phi_{fqr}||\Phi_{fqs}|$$

and:

$$b_{fsp} = \beta_{fsp} = \kappa_f \sigma_{sfp} |F_f|, \quad b_{fqs} = \beta_{fqs} = \kappa_f \sigma_{fqs} |F_f|,$$

with:

$$\sigma_{sfp} = \cos\zeta_{fsp} |\Phi_{fsp}|, \quad \sigma_{fqs} = \cos\zeta_{fqs} |\Phi_{fqs}|.$$

So the coefficients of the linear system (15) are, for an interior intermediary cell Q_f:

$$\begin{cases} A_f = \kappa_f \frac{|F_f|}{h_{fp}+h_{fq}}, \\ B_{fs} = 2\kappa_f \frac{\sigma_{sfp}+\sigma_{fqs}}{h_{fp}+h_{fq}}, \\ C_{fd} = 2\kappa_f \frac{\sigma_{frp}+\sigma_{fqr}-\sigma_{fup}-\sigma_{fqu}}{h_{fp}+h_{fq}}, \\ D_{fds} = 4\kappa_f \frac{1}{|F_f|} \Big(\frac{|\Phi_{fsp}|}{h_{fp}} (\cos\eta_{frps} |\Phi_{frp}| - \cos\eta_{fups} |\Phi_{fup}|) + \frac{|\Phi_{fqs}|}{h_{fq}} (\cos\eta_{fqrs} |\Phi_{fqr}| - \cos\eta_{fqus} |\Phi_{fqu}|) \\ \qquad -(h_{fq}\sigma_{sfp} - h_{fp}\sigma_{fqs}) \big(\frac{\sigma_{frp}-\sigma_{fup}}{h_{fp}(h_{fp}+h_{fq})} - \frac{\sigma_{fqr}-\sigma_{fqu}}{h_{fq}(h_{fp}+h_{fq})} \big) \Big), \end{cases}$$

and, for a boundary intermediary cell Q_f:

$$\begin{cases} A_f = \kappa_f \frac{|F_f|}{h_{fp}}, \\ B_{fs} = 2\kappa_f \frac{\sigma_{sfp}}{h_{fp}}, \\ C_{fd} = 2\kappa_f \frac{\sigma_{frp}-\sigma_{fup}}{h_{fp}}, \\ D_{fds} = 4\kappa_f \frac{|\Phi_{fsp}|}{h_{fp}}(\cos\eta_{frps}|\Phi_{frp}| - \cos\eta_{fups}|\Phi_{fup}|). \end{cases}$$

Suppose that $\theta_{fp} = \theta_{fq} = \theta_f$ (θ_f = angle between $\mathbf{n}_f$ and $\Sigma_f = \xi_p\xi_q$) and $h_f = h_{fp} + h_{fq} = \cos\theta_f|\Sigma_f|$. We obtain:

$$\begin{cases} A_f = \kappa_f \frac{|F_f|}{h_f}, \\ B_{fs} = 2\kappa_f \frac{\sigma_{sfp}+\sigma_{fqs}}{h_f}, \\ C_{fd} = 2\kappa_f \frac{\sigma_{frp}+\sigma_{fqr}-\sigma_{fup}-\sigma_{fqu}}{h_f}, \\ D_{fds} = 4\kappa_f \frac{1}{\cos\theta_f}\frac{1}{|F_f|}\left(\frac{|\Phi_{fsp}|}{|\Sigma_{fp}|}(\cos\eta_{frps}|\Phi_{frp}| - \cos\eta_{fups}|\Phi_{fup}|) + \frac{|\Phi_{fqs}|}{|\Sigma_{fq}|}(\cos\eta_{fqrs}|\Phi_{fqr}| - \cos\eta_{fqus}|\Phi_{fqu}|)\right. \\ \qquad \left. -(|\Sigma_{fq}|\sigma_{sfp} - |\Sigma_{fp}|\sigma_{fqs})\left(\frac{\sigma_{frp}-\sigma_{fup}}{|\Sigma_f||\Sigma_{fp}|} - \frac{\sigma_{fqr}-\sigma_{fqu}}{|\Sigma_f||\Sigma_{fq}|}\right)\right). \end{cases}$$

Finally, if $\theta_f = 0$, that is if the primal and dual meshes are perpendicular (this the case for Delaunay–Voronoi meshes or *admissible* meshes as defined in [45]), then, for all S_s, $\zeta_{fsp} = \zeta_{fqs} = 0$ (so $\sigma_{fsp} = \sigma_{fqs} = 0$), and we get:

$$\begin{cases} A_f = \kappa_f \frac{|F_f|}{h_f}, \\ B_{fs} = C_{fd} = 0, \\ D_{fds} = 4\kappa_f \frac{1}{|F_f|}\left(\frac{|\Phi_{fsp}|}{|\Sigma_{fp}|}(\cos\eta_{frps}|\Phi_{frp}| - \cos\eta_{fups}|\Phi_{fup}|) + \frac{|\Phi_{fqs}|}{|\Sigma_{fq}|}(\cos\eta_{fqrs}|\Phi_{fqr}| - \cos\eta_{fqus}|\Phi_{fqu}|)\right). \end{cases}$$

In this case the linear system (15) boils down to *two* independent systems, the first (resp. second) one having as unknowns the values of u at the primal (resp. dual) points.

For a *cube* mesh whose side length is h, we have:

$$A_f = \kappa_f h, \quad B_{fs} = C_{fd} = 0, \quad D_{fds} = \frac{1}{4}\kappa_f h \quad \text{or} \quad D_{fds} = -\frac{1}{4}\kappa_f h.$$

In this last case the system boils down to *three* independent linear systems, the first one having as unknowns the values of u at the primal points (see Fig. 10, left) and the last two ones having as unknowns the values of u at the dual points that are not linked with a side (black circles on the one hand and white circles on the other hand: see Fig. 10, right).

3.8. Link with the diamond-type schemes

Let N_d be the set of primal cells whose $\mathbf{x}_d$ is a vertex. By substituting to the third and fourth equation of (15) any formula which gives an approximation of the (dual) values u_d *from* the (primal) values u_p, for example:

$$u_d = \frac{\sum_{P_p\in N_d}|P_p|u_p}{\sum_{P_p\in N_d}|P_p|}$$

or:

$$u_d = \frac{\sum_{P_p\in N_d}|\xi_p\mathbf{x}_d|^{-1}u_p}{\sum_{P_p\in N_d}|\xi_p\mathbf{x}_d|^{-1}},$$

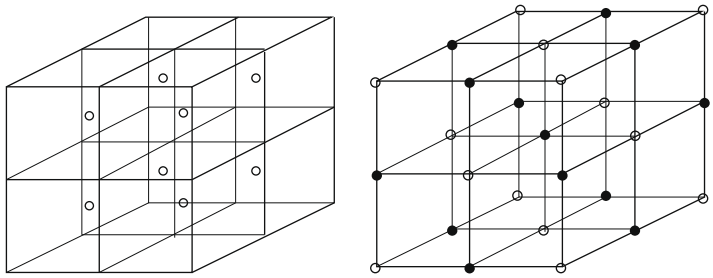

Fig. 10. *Left*: primal degrees of freedom. *Right*: dual degrees of freedom.

we obtain *diamond*-type schemes whose associated matrices are not symmetric (see [46–51] in two dimensions). Note that *non-linear* diamond-type methods have been recently devised in order to obtain monotone matrices (see [52–55]).

4. Numerical experiments

Given a scalar function u and its gradient $\mathbf{v} = \nabla u$, let us define the discrete L^2 (resp. L^∞)-norm by:

$$||u||_2 = \left(\frac{1}{2}\left(\sum_p |P_p| u_p^2 + \sum_d |\Pi_d| u_d^2\right)\right)^{\frac{1}{2}} \quad (\text{resp.} \quad ||u||_\infty = \max_{p,d}(u_p, u_d))$$

and:

$$||\mathbf{v}||_2 = \left(\sum_f |Q_f| \mathbf{v}_f \cdot \mathbf{v}_f\right)^{\frac{1}{2}} \quad (\text{resp.} \quad ||\mathbf{v}||_\infty = \max_f((\mathbf{v}_f \cdot \mathbf{v}_f)^{\frac{1}{2}})).$$

Let N be the number of cells and define by h the following characteristic length associated with the mesh of the domain Ω:

$$h = \left(\frac{|\Omega|}{N}\right)^{\frac{1}{3}}.$$

The relative error between the exact solution u_e (resp. gradient of the solution $\mathbf{v}_e = \nabla u_e$) and the approximated one u_h (resp. $\mathbf{v}_h = (\nabla u)_h$) are defined by:

$$e_2^h = \frac{||u_h - u_e||_2}{||u_e||_2}, \quad e_\infty^h = \frac{||u_h - u_e||_\infty}{||u_e||_\infty} \quad \left(e_2^h = \frac{||\mathbf{v}_h - \mathbf{v}_e||_2}{||\mathbf{v}_e||_2}, \quad e_\infty^h = \frac{||\mathbf{v}_h - \mathbf{v}_e||_\infty}{||\mathbf{v}_e||_\infty}\right).$$

The order of the method is given by:

$$\text{order} = \frac{\log(e^{2h}) - \log(e^h)}{\log 2}.$$

The large linear systems that arise from the implementation of the method are diagonally preconditioned before being solved by the conjugate gradient method when they are symmetric and by the BiCGSTAB method when they are not (see for example [56]). The stopping criterion for these methods is the relative decrease in the norm of the residual by a factor of 10^{-15}. The initial guess is always the unit vector.

In what follows Ω is the unit cube $[0,1]^3$. We have tested six groups of meshes of Ω.

1. Cube meshes from the coarsest (5^3 cells) to the finest (80^3 cells).
2. Tetrahedron meshes from the coarsest (6×5^3 cells) to the finest (6×80^3 cells), defined by dividing each cube of the previous meshes into six tetrahedra.
3. Randomly distorted hexahedron meshes from the coarsest (5^3 cells) to the finest (80^3 cells) which are made up by transforming the meshes of the first group by the maping:

$$\begin{cases} X = x + Chr_1, \\ Y = y + Chr_2, \\ Z = z + Chr_3, \end{cases} \tag{19}$$

   where $C = 0.4$, h is the length of the cube edges and r_1, r_2, r_3 are random numbers chosen between -1 and 1.
4. Randomly distorted tetrahedron meshes from the coarsest (6×5^3 cells) to the finest (6×80^3 cells) which are made up by transforming the meshes of the second group by the maping (19) with $C = 0.2$.
5. Continuously distorted hexahedron meshes from the coarsest (5^3 cells) to the finest (80^3 cells) which are made up by transforming the meshes of the first group by the maping (see [32]):

$$\begin{cases} X = x + 0.1\sin(2\pi x)\sin(2\pi y)\sin(2\pi z), \\ Y = y + 0.1\sin(2\pi x)\sin(2\pi y)\sin(2\pi z), \\ Z = z + 0.1\sin(2\pi x)\sin(2\pi y)\sin(2\pi z). \end{cases}$$

6. Distorted hexahedron meshes of *Kershaw*'s type, from the coarsest (10^3 cells, see Fig. 11) to the finest (80^3 cells).

For all these meshes, note that: $h^{-1} = 5\alpha, 10\alpha, 20\alpha, 40\alpha, 80\alpha$, with $\alpha = 6^{\frac{1}{3}}$ (tetrahedra) or $\alpha = 1$ (hexahedra).

4.1. First example: $\boldsymbol{\kappa}$ is a scalar tensor

Suppose that $\boldsymbol{\kappa}$ is the unit matrix and that f is such that $u = \sin(\pi x)\sin(\pi y)\sin(\pi z)$ is the solution to (1) with a Dirichlet boundary condition. The relative errors between the computed solution (resp. gradient of the solution) and the exact solution (resp. gradient of the solution) are given in Table 1 (resp. Table 2).

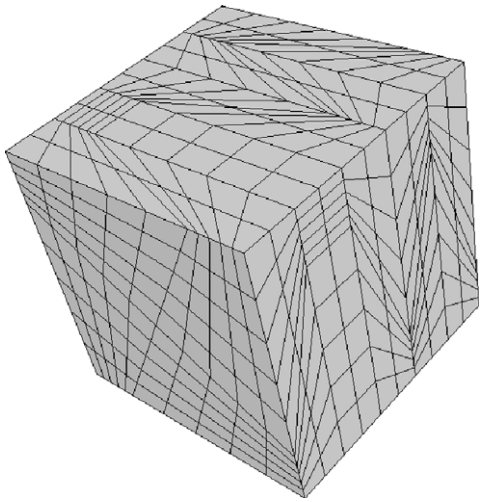

Fig. 11. The coarse distorted hexahedron mesh of the unit cube (10^3 cells).

Table 1
First example. Relative errors for u ($\alpha = 6^{\frac{1}{3}}$: tetrahedra, $\alpha = 1$: hexahedra).

h^{-1}	Cubes	Order	Regular tetrahedra	Order	Randomly hexahedra	Order
	e_2^h		e_2^h		e_2^h	
5α	1.03×10^{-1}		5.03×10^{-2}		1.26×10^{-1}	
10α	2.44×10^{-2}	2.08	1.17×10^{-2}	2.10	3.20×10^{-2}	1.97
20α	6.02×10^{-3}	2.02	3.71×10^{-3}	1.65	8.04×10^{-3}	1.99
40α	1.50×10^{-3}	2.00	8.26×10^{-4}	2.16	2.04×10^{-3}	1.98
80α	3.74×10^{-4}	2.00	1.91×10^{-4}	2.11	5.18×10^{-4}	1.98
	e_∞^h		e_∞^h		e_∞^h	
5α	1.23×10^{-1}		5.77×10^{-2}		2.17×10^{-1}	
10α	3.35×10^{-2}	1.87	1.54×10^{-2}	1.95	5.87×10^{-2}	1.89
20α	8.26×10^{-3}	2.02	6.72×10^{-3}	1.19	1.52×10^{-2}	1.94
40α	2.06×10^{-3}	2.00	2.05×10^{-3}	1.71	3.92×10^{-3}	1.95
80α	5.14×10^{-4}	2.00	5.23×10^{-4}	1.97	1.09×10^{-3}	1.85

h^{-1}	Randomly tetrahedra	Order	Continuously distorted hexahedra	Order	Distorted hexahedra	Order
	e_2^h		e_2^h		e_2^h	
5α	5.36×10^{-2}		1.23×10^{-1}			
10α	1.22×10^{-2}	2.13	3.13×10^{-2}	1.97	2.56×10^{-2}	
20α	3.88×10^{-3}	1.66	7.99×10^{-3}	1.97	6.66×10^{-3}	1.99
40α	8.74×10^{-4}	2.15	2.01×10^{-3}	1.99	1.62×10^{-3}	2.00
80α	2.03×10^{-4}	2.11	5.03×10^{-4}	2.00	4.05×10^{-4}	2.00
	e_∞^h		e_∞^h		e_∞^h	
5α	7.88×10^{-2}		1.33×10^{-1}			
10α	1.71×10^{-2}	2.20	3.56×10^{-2}	1.91	3.09×10^{-2}	
20α	6.69×10^{-3}	1.35	9.21×10^{-3}	1.93	7.70×10^{-3}	2.00
40α	2.13×10^{-3}	1.65	2.32×10^{-3}	2.00	1.92×10^{-3}	2.00
80α	5.61×10^{-4}	1.92	5.80×10^{-4}	2.00	4.80×10^{-4}	2.00

4.2. Second example: $\boldsymbol{\kappa}$ is a full anisotropic symmetric tensor

Suppose that $\boldsymbol{\kappa} = \boldsymbol{\kappa}(\mathbf{x})$ is the symmetric positive definite matrix defined by:

$$\boldsymbol{\kappa} = \begin{pmatrix} \cos\pi x & -\sin\pi x & 0 \\ \sin\pi x & \cos\pi x & 0 \\ 0 & 0 & 1 \end{pmatrix} \begin{pmatrix} 1 & 0 & 0 \\ 0 & \varepsilon & 0 \\ 0 & 0 & \eta(1+x+y+z) \end{pmatrix} \begin{pmatrix} \cos\pi x & \sin\pi x & 0 \\ -\sin\pi x & \cos\pi x & 0 \\ 0 & 0 & 1 \end{pmatrix} \tag{20}$$

and let f be the function such that $u = \sin(\pi x)\sin(\pi y)\sin(\pi z)$ is the solution to (1) with a Dirichlet boundary condition. We have chosen $\varepsilon = 10^{-1}$ and $\eta = 10$. This test is a 3D extension of a plasma physics benchmark coming from [57]. The relative

Table 2
First example. Relative errors for ∇u ($\alpha = 6^{\frac{1}{3}}$: tetrahedra, $\alpha = 1$: hexahedra).

h^{-1}	Cubes	Order	Regular tetrahedra	Order	Randomly hexahedra	Order
	e_2^h		e_2^h		e_2^h	
5α	5.71×10^{-2}		2.26×10^{-1}		1.23×10^{-1}	
10α	1.38×10^{-2}	2.05	1.11×10^{-1}	1.02	5.18×10^{-2}	1.25
20α	3.42×10^{-3}	2.01	5.18×10^{-2}	1.11	2.48×10^{-2}	1.06
40α	8.53×10^{-4}	2.00	2.70×10^{-2}	0.94	1.23×10^{-2}	1.02
80α	2.13×10^{-4}	2.00	1.38×10^{-2}	0.97	6.16×10^{-3}	0.99
	e_∞^h		e_∞^h		e_∞^h	
5α	6.24×10^{-2}		2.95×10^{-1}		2.36×10^{-1}	
10α	1.66×10^{-2}	1.91	1.58×10^{-1}	0.91	1.60×10^{-1}	0.56
20α	4.12×10^{-3}	2.01	7.38×10^{-2}	1.09	7.51×10^{-2}	1.09
40α	1.03×10^{-3}	2.00	4.05×10^{-2}	0.87	4.97×10^{-2}	0.59
80α	2.57×10^{-4}	2.00	2.04×10^{-2}	0.99	3.64×10^{-2}	0.45

h^{-1}	Randomly tetrahedra	Order	Continuously distorted hexahedra	Order	Distorted hexahedra	Order
	e_2^h		e_2^h		e_2^h	
5α	2.28×10^{-1}		1.12×10^{-1}			
10α	1.17×10^{-1}	0.96	3.17×10^{-2}	1.82	2.27×10^{-2}	
20α	5.49×10^{-2}	1.09	8.25×10^{-3}	1.94	5.85×10^{-3}	1.92
40α	2.87×10^{-2}	0.94	2.09×10^{-3}	1.98	1.48×10^{-3}	1.98
80α	1.46×10^{-2}	0.97	5.24×10^{-4}	1.99	3.71×10^{-4}	1.99
	e_∞^h		e_∞^h		e_∞^h	
5α	3.40×10^{-1}		1.33×10^{-1}			
10α	2.47×10^{-1}	0.46	4.35×10^{-2}	1.60	4.64×10^{-2}	
20α	1.23×10^{-1}	1.00	1.37×10^{-2}	1.66	1.60×10^{-2}	1.53
40α	8.35×10^{-2}	0.56	1.95×10^{-3}	1.79	5.63×10^{-3}	1.50
80α	4.64×10^{-2}	0.85	1.04×10^{-3}	1.93	2.06×10^{-3}	1.45

Table 3
Second example. Relative errors for u ($\alpha = 6^{\frac{1}{3}}$: tetrahedra, $\alpha = 1$: hexahedra).

h^{-1}	Cubes	Order	Regular tetrahedra	Order	Randomly hexahedra	Order
	e_2^h		e_2^h		e_2^h	
5α	1.03×10^{-1}		6.66×10^{-2}		1.48×10^{-1}	
10α	2.43×10^{-2}	2.08	1.62×10^{-2}	2.03	4.25×10^{-2}	1.80
20α	5.99×10^{-3}	2.02	4.85×10^{-3}	1.74	1.01×10^{-2}	2.07
40α	1.49×10^{-3}	2.00	1.21×10^{-3}	1.99	2.60×10^{-3}	1.96
80α	3.73×10^{-4}	2.00	2.82×10^{-4}	2.10	6.64×10^{-4}	1.97
	e_∞^h		e_∞^h		e_∞^h	
5α	1.23×10^{-1}		7.01×10^{-2}		2.61×10^{-1}	
10α	3.31×10^{-2}	1.91	1.89×10^{-2}	1.89	7.64×10^{-2}	1.77
20α	8.15×10^{-3}	2.02	7.71×10^{-3}	1.29	2.26×10^{-2}	1.76
40α	2.03×10^{-3}	2.00	2.90×10^{-3}	1.41	5.49×10^{-3}	2.04
80α	5.08×10^{-4}	2.00	7.83×10^{-4}	1.89	1.74×10^{-3}	1.65

h^{-1}	Randomly tetrahedra	Order	Continuously distorted hexahedra	Order	Distorted hexahedra	Order
	e_2^h		e_2^h		e_2^h	
5α	7.63×10^{-2}		1.47×10^{-1}			
10α	1.94×10^{-2}	1.97	3.56×10^{-2}	2.04	3.01×10^{-2}	
20α	5.63×10^{-3}	1.78	8.90×10^{-3}	2.00	7.36×10^{-3}	2.03
40α	1.38×10^{-3}	2.02	2.22×10^{-3}	2.00	1.78×10^{-3}	2.04
80α	3.32×10^{-4}	2.06	5.57×10^{-4}	2.00	4.40×10^{-4}	2.02
	e_∞^h		e_∞^h		e_∞^h	
5α	1.32×10^{-1}		1.96×10^{-1}			
10α	2.75×10^{-2}	2.26	5.33×10^{-2}	1.88	4.68×10^{-2}	
20α	1.04×10^{-2}	1.40	1.40×10^{-2}	1.92	1.17×10^{-2}	2.03
40α	2.88×10^{-3}	1.85	3.48×10^{-3}	2.01	3.52×10^{-3}	2.04
80α	7.99×10^{-4}	1.85	8.70×10^{-4}	2.00	9.29×10^{-4}	2.02

errors between the computed solution (resp. gradient of the solution) and the exact solution (resp. gradient of the solution) are given in Table 3 (resp. Table 4).

4.3. Third example: $\boldsymbol{\kappa}$ is an antisymmetric tensor

Suppose that $\boldsymbol{\kappa} = \boldsymbol{\kappa}(\mathbf{x})$ is the antisymmetric positive definite matrix defined by:

Table 4
Second example. Relative errors for ∇u ($\alpha = 6^{\frac{1}{3}}$: tetrahedra, $\alpha = 1$: hexahedra).

h^{-1}	Cubes	Order	Regular tetrahedra	Order	Randomly hexahedra	Order
	e_2^h		e_2^h		e_2^h	
5α	5.81×10^{-2}		2.59×10^{-1}		1.96×10^{-1}	
10α	1.41×10^{-2}	2.05	1.26×10^{-1}	1.04	1.07×10^{-1}	0.89
20α	3.49×10^{-3}	2.00	5.97×10^{-2}	1.08	4.60×10^{-2}	1.20
40α	8.71×10^{-4}	2.00	3.16×10^{-2}	0.92	2.24×10^{-2}	1.04
80α	2.18×10^{-4}	2.00	1.57×10^{-2}	1.00	1.12×10^{-2}	1.00
	e_∞^h		e_∞^h		e_∞^h	
5α	7.71×10^{-2}		3.78×10^{-1}		6.56×10^{-1}	
10α	2.16×10^{-2}	1.83	2.09×10^{-1}	0.85	4.12×10^{-1}	0.67
20α	5.63×10^{-3}	1.94	1.08×10^{-1}	0.95	2.32×10^{-1}	0.82
40α	1.46×10^{-3}	1.94	7.49×10^{-2}	0.53	1.15×10^{-1}	1.00
80α	3.77×10^{-4}	1.95	4.07×10^{-2}	0.88	7.54×10^{-2}	0.61

h^{-1}	Randomly tetrahedra	Order	Continuously distorted hexahedra	Order	Distorted hexahedra	Order
	e_2^h		e_2^h		e_2^h	
5α	2.71×10^{-1}		1.84×10^{-1}			
10α	1.40×10^{-1}	0.95	5.46×10^{-2}	1.75	7.15×10^{-2}	
20α	6.69×10^{-2}	1.07	1.47×10^{-2}	1.89	2.51×10^{-2}	1.51
40α	3.52×10^{-2}	0.93	3.76×10^{-3}	1.96	7.44×10^{-3}	1.76
80α	1.78×10^{-2}	0.98	9.47×10^{-4}	1.99	1.97×10^{-3}	1.91
	e_∞^h		e_∞^h		e_∞^h	
5α	4.61×10^{-1}		4.05×10^{-1}			
10α	3.47×10^{-1}	0.41	1.63×10^{-1}	1.31	2.32×10^{-2}	
20α	2.04×10^{-1}	0.77	5.51×10^{-2}	1.57	1.15×10^{-3}	1.01
40α	1.20×10^{-1}	0.76	1.68×10^{-2}	1.72	4.38×10^{-4}	1.40
80α	5.95×10^{-2}	1.01	5.51×10^{-3}	1.61	1.45×10^{-4}	1.60

Table 5
Third example. Relative errors for u ($\alpha = 6^{\frac{1}{3}}$: tetrahedra, $\alpha = 1$: hexahedra).

h^{-1}	Cubes	Order	Regular tetrahedra	Order	Randomly hexahedra	Order
	e_2^h		e_2^h		e_2^h	
5α	1.03×10^{-1}		5.04×10^{-2}		1.27×10^{-1}	
10α	2.44×10^{-2}	2.08	1.17×10^{-2}	2.10	3.21×10^{-2}	1.98
20α	6.02×10^{-3}	2.02	3.73×10^{-3}	1.65	8.03×10^{-3}	1.99
40α	1.50×10^{-3}	2.00	8.34×10^{-4}	2.16	2.04×10^{-3}	1.97
80α	3.74×10^{-4}	2.00	1.93×10^{-4}	2.11	5.19×10^{-4}	1.98
	e_∞^h		e_∞^h		e_∞^h	
5α	1.23×10^{-1}		5.95×10^{-2}		2.00×10^{-1}	
10α	3.35×10^{-2}	1.87	1.54×10^{-2}	1.95	5.88×10^{-2}	1.77
20α	8.26×10^{-3}	2.02	6.73×10^{-3}	1.19	1.46×10^{-2}	2.01
40α	2.06×10^{-3}	2.00	2.05×10^{-3}	1.71	3.87×10^{-3}	1.91
80α	5.14×10^{-4}	2.00	5.24×10^{-4}	1.97	1.09×10^{-3}	1.83

h^{-1}	Randomly tetrahedra	Order	Continuously distorted hexahedra	Order	Distorted hexahedra	Order
	e_2^h		e_2^h		e_2^h	
5α	5.46×10^{-2}		1.23×10^{-1}			
10α	1.22×10^{-2}	2.15	3.13×10^{-2}	1.97	2.61×10^{-2}	
20α	3.92×10^{-3}	1.64	7.98×10^{-3}	1.97	6.56×10^{-3}	1.99
40α	8.86×10^{-4}	2.14	2.01×10^{-3}	1.99	1.64×10^{-3}	2.00
80α	2.04×10^{-4}	2.11	5.03×10^{-4}	2.00	4.10×10^{-4}	2.00
	e_∞^h		e_∞^h		e_∞^h	
5α	7.77×10^{-2}		1.35×10^{-1}			
10α	1.69×10^{-2}	2.20	3.58×10^{-2}	1.92	3.15×10^{-2}	
20α	6.82×10^{-3}	1.30	9.26×10^{-3}	1.95	7.86×10^{-3}	2.00
40α	2.14×10^{-3}	1.67	2.31×10^{-3}	2.00	1.96×10^{-3}	2.00
80α	5.61×10^{-4}	1.94	5.78×10^{-4}	2.00	4.90×10^{-4}	2.00

$$\boldsymbol{\kappa} = \begin{pmatrix} 1 & 1+xy & 1+xz \\ -1-xy & 1 & 1+yz \\ -1-xz & -1-yz & 1 \end{pmatrix}$$

Table 6
Third example. Relative errors for $\mathbf{V}u$ ($\alpha = 6^{\frac{1}{3}}$: tetrahedra, $\alpha = 1$: hexahedra).

h^{-1}	Cubes	Order	Regular tetrahedra	Order	Randomly hexahedra	Order
	e_2^h		e_2^h		e_2^h	
5α	5.71×10^{-2}		2.26×10^{-1}		1.25×10^{-1}	
10α	1.38×10^{-2}	2.05	1.11×10^{-1}	1.02	5.22×10^{-2}	1.26
20α	3.42×10^{-3}	2.01	5.18×10^{-2}	1.11	2.50×10^{-2}	1.06
40α	8.53×10^{-4}	2.00	2.70×10^{-2}	0.94	1.23×10^{-2}	1.02
80α	2.13×10^{-4}	2.00	1.38×10^{-2}	0.97	6.19×10^{-3}	0.99
	e_∞^h		e_∞^h		e_∞^h	
5α	6.30×10^{-2}		2.97×10^{-1}		2.54×10^{-1}	
10α	1.70×10^{-2}	1.89	1.57×10^{-1}	0.92	1.65×10^{-1}	0.62
20α	4.23×10^{-3}	2.00	7.43×10^{-2}	1.08	7.47×10^{-2}	1.14
40α	1.06×10^{-3}	2.00	4.06×10^{-2}	0.87	4.91×10^{-2}	0.60
80α	2.65×10^{-4}	2.00	2.04×10^{-2}	0.99	3.67×10^{-2}	0.42
h^{-1}	Randomly tetrahedra	Order	Continuously distorted hexahedra	Order	Distorted hexahedra	Order
	e_2^h		e_2^h		e_2^h	
5α	2.28×10^{-1}		1.13×10^{-1}			
10α	1.17×10^{-1}	0.96	3.18×10^{-2}	1.82	2.32×10^{-2}	
20α	5.50×10^{-2}	1.08	8.30×10^{-3}	1.94	6.03×10^{-3}	1.94
40α	2.87×10^{-2}	0.94	2.10×10^{-3}	1.98	1.56×10^{-3}	1.95
80α	1.46×10^{-2}	0.97	5.27×10^{-4}	1.99	4.07×10^{-4}	1.94
	e_∞^h		e_∞^h		e_∞^h	
5α	3.40×10^{-1}		1.37×10^{-1}			
10α	2.48×10^{-1}	0.45	4.67×10^{-2}	1.55	5.22×10^{-2}	
20α	1.21×10^{-1}	1.03	1.53×10^{-2}	1.61	1.88×10^{-2}	1.47
40α	8.28×10^{-2}	0.55	4.28×10^{-3}	1.83	7.23×10^{-3}	1.38
80α	4.65×10^{-2}	0.83	1.11×10^{-3}	1.95	2.57×10^{-3}	1.49

Table 7
Fourth example. Relative errors for u ($\alpha = 6^{\frac{1}{3}}$: tetrahedra, $\alpha = 1$: hexahedra).

h^{-1}	Cubes	Order	Regular tetrahedra	Order	Randomly hexahedra	Order
	e_2^h		e_2^h		e_2^h	
10α	2.83×10^{-4}		2.88×10^{-4}		7.95×10^{-4}	
20α	7.44×10^{-5}	1.93	1.11×10^{-4}	1.37	2.36×10^{-4}	1.75
40α	1.89×10^{-5}	1.98	2.62×10^{-5}	2.08	6.25×10^{-5}	1.91
80α	4.75×10^{-6}	1.99	6.09×10^{-6}	2.10	1.67×10^{-5}	1.91
	e_∞^h		e_∞^h		e_∞^h	
10α	4.64×10^{-4}		5.57×10^{-4}		1.53×10^{-3}	
20α	1.34×10^{-4}	1.79	1.53×10^{-4}	1.85	5.63×10^{-4}	1.45
40α	3.75×10^{-5}	1.84	5.66×10^{-5}	1.44	1.65×10^{-4}	1.77
80α	1.00×10^{-5}	1.90	1.61×10^{-5}	1.81	5.31×10^{-5}	1.64
h^{-1}	Randomly tetrahedra	Order	Continuously distorted hexahedra	Order	Distorted hexahedra	Order
	e_2^h		e_2^h		e_2^h	
10α	3.34×10^{-4}		6.69×10^{-4}		1.42×10^{-3}	
20α	1.26×10^{-4}	1.40	1.88×10^{-4}	1.83	3.69×10^{-4}	1.95
40α	3.08×10^{-5}	2.03	4.88×10^{-5}	1.95	9.34×10^{-5}	1.98
80α	7.21×10^{-6}	2.09	1.23×10^{-5}	1.98	2.35×10^{-5}	1.99
	e_∞^h		e_∞^h		e_∞^h	
10α	7.57×10^{-4}		1.40×10^{-3}		2.82×10^{-3}	
20α	2.31×10^{-4}	1.71	4.88×10^{-4}	1.52	9.92×10^{-4}	1.51
40α	7.80×10^{-5}	1.56	1.43×10^{-4}	1.77	3.14×10^{-4}	1.66
80α	2.14×10^{-5}	1.87	3.85×10^{-5}	1.90	9.18×10^{-5}	1.77

and let f be the function such that $u = \sin(\pi x)\sin(\pi y)\sin(\pi z)$ is the solution to (1) with a Dirichlet boundary condition. This test is a 3D extension of a benchmark coming from [3]. The relative errors between the computed solution (resp. gradient of the solution) and the exact solution (resp. gradient of the solution) are given in Table 5 (resp. Table 6).

4.4. Fourth example: $\boldsymbol{\kappa}$ is discontinuous

Suppose that $\boldsymbol{\kappa} = \boldsymbol{\kappa}(\mathbf{x})$ is the positive definite matrix defined by:

$$\boldsymbol{\kappa} = \begin{pmatrix} 1 & 0 & 0 \\ 0 & 1 & 0 \\ 0 & 0 & 1 \end{pmatrix} \quad \text{if } x \leqslant 0.5$$

and:

$$\boldsymbol{\kappa} = \begin{pmatrix} 2 & 1 & 0 \\ 1 & 2 & 0 \\ 0 & 0 & 1 \end{pmatrix} \quad \text{if } x > 0.5.$$

Let f be the function such that:

$$\begin{cases} u = (x - 0.5)(2\sin y + \cos y) + \sin y + z & \text{if} \quad x \leqslant 0.5, \\ u = e^{x-0.5}\sin y + z & \text{if } x > 0.5, \end{cases}$$

is the solution to (1). If $x = 0.5$ and $\mathbf{n} = (1,0,0)$, note that $(\boldsymbol{\kappa}\nabla u)\cdot\mathbf{n} = 2\sin y + \cos y$. This test is a 3D extension of a benchmark inspired from [58]. Note that all the meshes we have tested honour the discontinuity plane $x = 0.5$. The relative errors between the computed solution and the exact solution are given in Table 7.

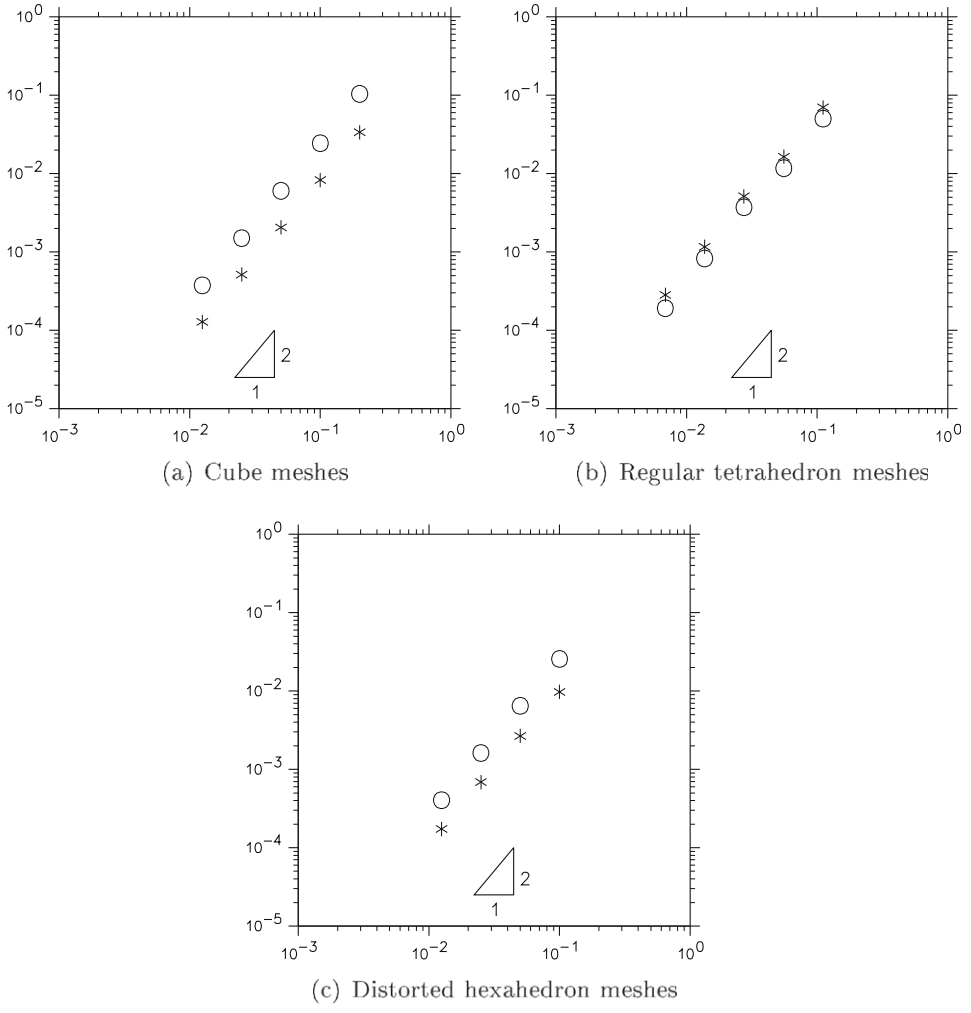

Fig. 12. *First example*. Errors in the L^2-norm for u with the old ($*$) and new ($\bigcirc$) methods.

4.5. Discussion

The previous numerical experiments call several remarks. For *all* the benchmarks and for *all* the meshes considered, we have observed a second-order (resp. nearly second-order) convergence rate in the L^2 (resp. L^∞) norm for u. Regarding ∇u, we have observed, for *all* the benchmarks:

- a second-order (resp. nearly second order) convergence rate in the L^2 (resp. L^∞) norm for the cube mesh,
- a convergence rate between 1.5 and 2 in the L^2 (resp. L^∞) norm for all the hexahedron meshes except the randomly mesh,
- a first-order (resp. nearly first-order) convergence rate in the L^2 (resp. L^∞) norm for the randomly hexahedron mesh and for all the tetrahedron meshes.

Comparisons between the *old* method described in [10] and the *new* proposed method have been carried out for the cube, regular tetrahedron and distorted hexahedron meshes: see Figs. 12–14. For hexahedron meshes the old method is slightly more precise but it fails to converge when continuously distorted and randomly meshes are used or when highly anisotropic diffusion tensors have to be dealt with (this is the reason for which some values "☆", standing for the numerical result with the old method, are lacking on Fig. 13).

The new method is more robust since it converges for all the type of meshes we have experimented so far. However handling highly anisotropic diffusion tensors of type (20) such that $\varepsilon \leqslant 10^{-6}\eta$ can deteriorate the convergence properties when distorted meshes are involved, as it has been already remarked for the 2D case: see [59]. Using right parallelepiped meshes seems to remain necessary for such difficult issues: note that an anisotropic diffusion tensor of type (20) with $\varepsilon \leqslant 10^{-16}\eta$ has been handled successfully when using a cube mesh.

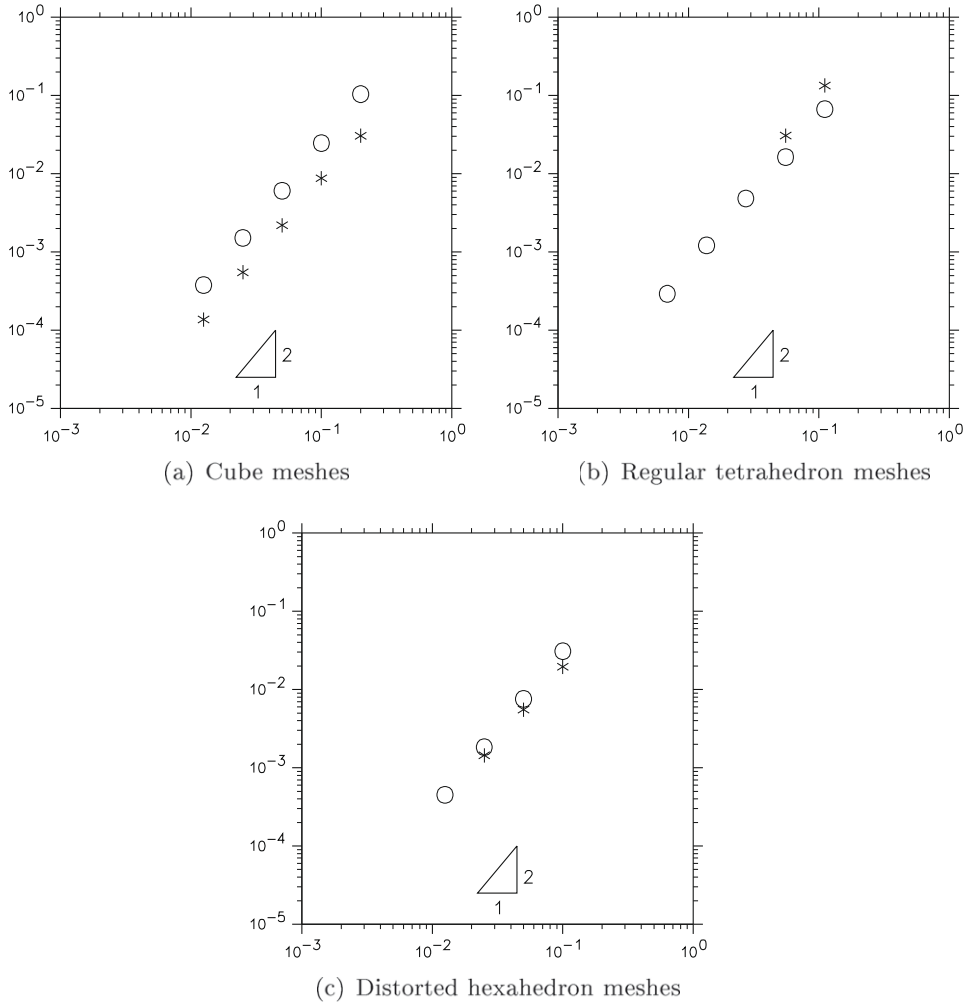

Fig. 13. *Second example*. Errors in the L^2-norm for u with the old ($*$) and new ($\bigcirc$) methods.

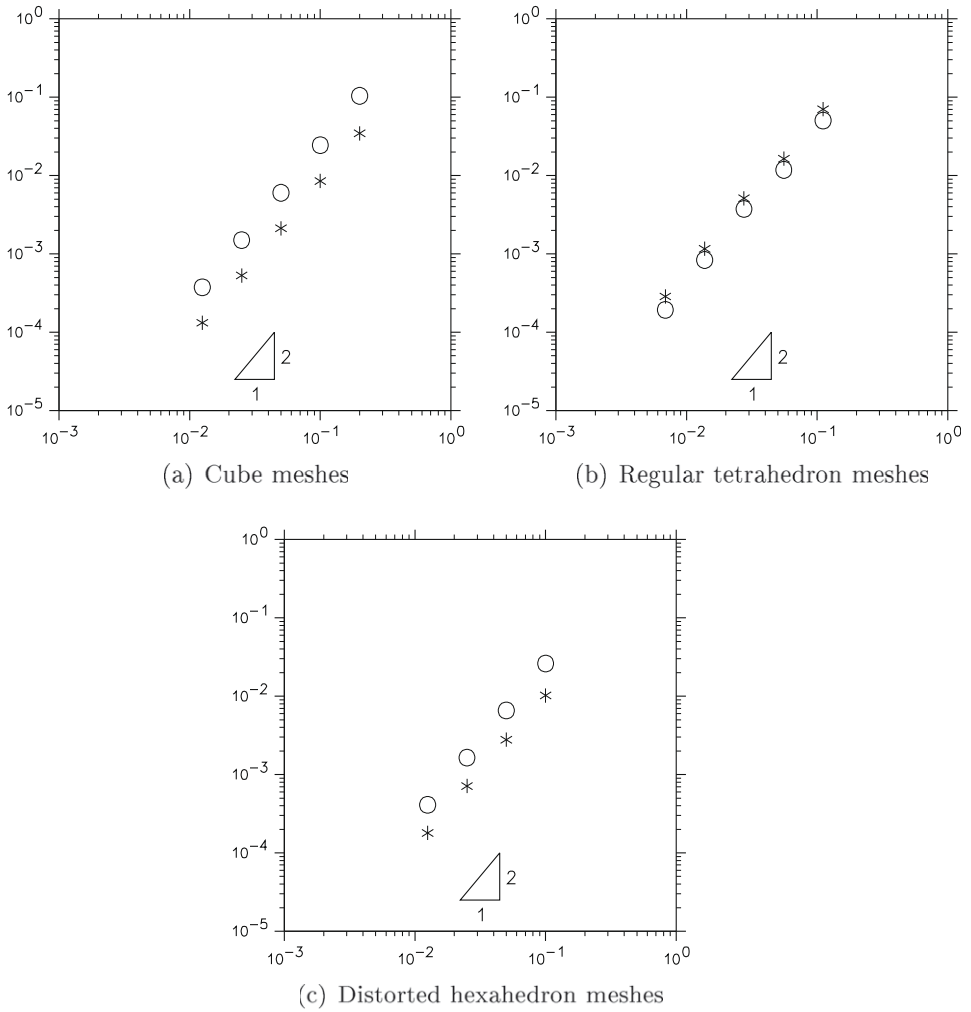

Fig. 14. *Third example*. Errors in the L^2-norm for u with the old ($*$) and new ($\bigcirc$) methods.

5. Concluding remarks

The numerical results presented in the paper demonstrate that the "new" proposed method is quite both robust and accurate when applied to general diffusion equations on general meshes. Comparisons with the "old" method proposed in [10] show a very clear improvement regarding the robustness. Extensive numerical comparisons between these methods and other ones (mixed hybrid finite element, control-volume multi-point-flux approximation, mimetic finite differences, discontinuous Galerkin,...), like those which have been carried out in the 2D case (see [25]), would be welcome. They will be the subject of future works.

Acknowledgments

The author is grateful to the referees for their valuable suggestions.

References

[1] F. Hermeline, Une méthode de volumes finis pour leséquations elliptiques du second ordre (in French), C.R. Acad. Sci. Paris Ser. 1 326 (1998) 1433–1436.
[2] F. Hermeline, A finite volume method for the approximation of diffusion operators on distorted meshes, J. Comput. Phys. 160 (2000) 481–499.
[3] F. Hermeline, Approximation of diffusion operators with discontinuous tensor coefficients on distorted meshes, Comput. Meth. Appl. Mech. Eng. 192 (2003) 1939–1959.
[4] F. Hermeline, A finite volume method for solving Maxwell equations in inhomogeneous media on arbitrary meshes, C.R. Acad. Sci. Paris Ser. 1 339 (2004) 893–898.
[5] K. Domelevo, P. Omnes, A finite volume method for the Laplace equation on almost arbitrary two-dimensional grids, Math. Model. Numer. Anal. 39 (2005) 1203–1249.

[6] S. Delcourte, K. Domelevo, P. Omnes, Discrete duality finite volume method for second order elliptic problems, in: F. Benkhaldoun, D. Ouazar, S. Raghay (Eds.), Finite Volumes for Complex Applications (IV), Hermes Science Publishing, 2005, pp. 447–458.
[7] B. Andreianov, F. Boyer, F. Hubert, Duplex finite volume schemes for nonlinear elliptic problems on general 2D meshes, in: F. Benkhaldoun, D. Ouazar, S. Raghay (Eds.), Finite Volumes for Complex Applications (IV), Hermes Science Publishing, 2005, pp. 365–375.
[8] C. Pierre, Modélisation et simulation de l'activité électrique du cœur dans le thorax, analyse numérique et méthodes de volumes finis (in French), Ph.D. Thesis, University of Nantes, France, 2005.
[9] A. Njifenjou, I.M. Nguena, A finite volume method for second order elliptic problems, Int. J. Finite Volume 3 (2) (2006).
[10] F. Hermeline, Approximation of 2-D and 3-D diffusion operators with variable full tensor coefficients on arbitrary meshes, Comput. Meth. Appl. Mech. Eng. 196 (2007) 2497–2526.
[11] B. Andreianov, F. Boyer, F. Hubert, Discrete duality finite volume schemes for Leray–Lions-type elliptic problems on general 2D meshes, Numer. Meth. Part. Differ. Equations 23 (1) (2007) 145–195.
[12] G. Yuan, Z. Sheng, Analysis of accuracy of a finite volume scheme for diffusion equations on distorted meshes, J. Comput. Phys. 220 (2007) 751–771.
[13] S. Delcourte, K. Domelevo, P. Omnes, A discrete duality finite volume approach to Hodge decomposition and div–curl problems on almost arbitrary two-dimensional meshes, SIAM J. Numer. Anal. 45 (3) (2007) 1142–1174.
[14] S. Delcourte, Développement de méthodes de volumes finis pour la mécanique des fluides (in French), Ph.D. Thesis, University of Toulouse, France, 2007.
[15] F. Hermeline, Approximating second order vector differential operators on distorted meshes in two space dimensions, Int. J. Numer. Meth. Eng. 76 (2008) 1065–1089.
[16] F. Hermeline, S. Layouni, P. Omnes, A finite volume method for the approximation of Maxwell's equations in two space dimensions on arbitrary meshes, J. Comput. Phys. 227 (2008) 9365–9388.
[17] F. Boyer, F. Hubert, Finite volume method for non linear transmission problems, in: Domain Decomposition Methods in Science and Engineering XVII, Lecture Notes in Computational Science and Engineering, vol. 60, Springer, Berlin, Heidelberg, 2008, pp. 443–450.
[18] A. Njifenjou, A.J. Kinfack, Convergence analysis of an MPFA method for flow problems in anisotropic heterogeneous porous media, Int. J. Finite Volume 5 (1) (2008).
[19] Y. Coudière, C. Pierre, O. Rousseau, R. Turpault, 2D/3D discrete duality finite volume scheme (DDFV) applied to ECG simulation, in: R. Eymard, J.M. Herard (Eds.), Finite Volumes for Complex Applications (V), Wiley, 2008, pp. 313–320.
[20] F. Boyer, F. Hubert, The DDFV "discrete duality finite volumes" and m-DDFV schemes, in: R. Eymard, J.M. Herard (Eds.), Finite Volumes for Complex Applications (V), Wiley, 2008, pp. 735–750.
[21] D. Calhoun, A finite volume discretization of the surface Laplacian for general curved, logically Cartesian meshes, 2008, personal communication.
[22] C. Chainais-Hillairet, Discrete duality finite volume schemes for two-dimensional drift-diffusion and energy-transport models, Int. J. Numer. Meth. Fluids 59 (2009) 239–257.
[23] Y. Coudière, F. Hubert, A 3D discrete duality finite volume method for non linear elliptic problem, in: A. Handlovicova, P. Frolkovic, K. Mikula, D. Sevcovic (Eds.), Proceedings of Algoritmy 2009, 2009, pp. 51–60.
[24] B. Andreianov, M. Bendahmane, On finite volume discretizations of gradient and divergence operators in the 3D case, HAL:hal00355212, 2009.
[25] R. Herbin, F. Hubert, Benchmark on discretization schemes for anisotropic diffusion problems on general grids, in: R. Eymard, J.M. Herard (Eds.), Finite Volumes for Complex Applications (V), Wiley, 2008, pp. 659–692.
[26] R.A. Klausen, T.F. Russel, Relationships among some locally conservative discretization methods which handle discontinuous coefficients, Comput. Geosci. 8 (2004) 341–377.
[27] H.A. Friis, M.G. Edwards, J. Mykkeltveit, Symmetric positive definite flux-continuous full-tensor finite-volume schemes on unstructured cell-centered triangular grids, SIAM J. Sci. Comput. 31 (2008) 1192–1220.
[28] A. Younes, V. Fontaine, Efficiency of mixed hybrid finite element and MPFA methods on quadrangular grids and highly anisotropic media, Int. J. Numer. Meth. Eng. (2008), doi:10.1002/nme.2327.
[29] A. Younes, V. Fontaine, Hybrid and multi-point formulations of the lowest-order mixed methods for Darcy's flow on triangles, Int. J. Numer. Meth. Fluids (2008), doi:10.1002/fld.785.
[30] Y. Kuznetsov, S. Repin, New mixed finite element method on polygonal and polyhedral meshes, Russ. J. Numer. Anal. Math. Model. 18 (3) (2003) 261–278.
[31] A. Bermudez, P. Gamallo, M.R. Nogueiras, R. Rodriguez, Approximation properties of lowest-order hexahedral Raviart-Thomas finite elements, C.R. Acad. Sci. Paris Ser. 1 340 (2005) 687–692.
[32] K. Lipnikov, M. Shashkov, D. Svyatskiy, The mimetic finite difference discretization of diffusion problem on unstructured polyhedral meshes, J. Comput. Phys. 211 (2006) 473–491.
[33] F. Brezzi, K. Lipnikov, M. Shashkov, V. Simoncini, A new discretization methodology for diffusion problems on generalized polyhedral meshes, Comput. Meth. Appl. Mech. Eng. 196 (2007) 3682–3692.
[34] J.E. Aarnes, S. Krogstad, K.A. Lie, Multiscale mixed/mimetic methods on corner-point grids, Comput. Geosci. 12 (2008) 297–315.
[35] Q.Y. Chen, J. Wan, Y. Yang, R.T. Mifflin, Enriched multi-point flux approximation for general grids, J. Comput. Phys. 227 (2008) 1701–1721.
[36] M. Fatenejad, G.A. Moses, Extension of Kershaw diffusion scheme to hexahedral meshes, J. Comput. Phys. 227 (2008) 2184–2187.
[37] T.S. Bailey, M.L. Adams, B. Yang, M.R. Zika, A piecewise linear finite element discretization of the diffusion equation for arbitrary polyhedral grids, J. Comput. Phys. 227 (2008) 3738–3757.
[38] G. Voronoi, Nouvelles applications des paramètres continusà la théorie des formes quadratiques: recherche sur les paralléllоèdres primitifs (in french), J. Reine Angew. Math. 134 (1908) 97–178.
[39] B. Delaunay, Sur la sphère vide (in french), Bul. Acad. Sci. URSS Class. Sci. Nat. (1934) 793–800.
[40] F. Hermeline, Une méthode automatique de maillage en dimension N (in french), Ph.D. Thesis, University P. and M. Curie Paris 6, Paris, 1980.
[41] F. Hermeline, Triangulation automatique d'un polyèdre en dimension N (in french), RAIRO Anal. Numér. 16 (1982) 211–242.
[42] P.L. George, F. Hermeline, Delaunay's mesh of a convex polyhedron in dimension d. Application to arbitrary polyhedra, Int. J. Numer. Meth. Eng. 33 (1992) 975–995.
[43] P.L. George, Automatic mesh generation and finite element computation, in: P.G. Ciarlet, J.L. Lions (Eds.), Handbook of Numerical Analysis, vol. 7, North Holland, Elsevier, 1996, pp. 713–1018.
[44] P.J. Frey, P.L. George, Mesh Generation, Hermes Science Publishing, 2000.
[45] R. Eymard, T. Gallouet, R. Herbin, Finite volume methods, in: P.G. Ciarlet, J.L. Lions (Eds.), Handbook of Numerical Analysis, vol. 7, North Holland, 2000.
[46] W.J. Coirier, An adaptively-refined Cartesian, cell-based scheme for the Euler and Navier–Stokes equations, Ph.D. Thesis, Michigan University, 1994.
[47] Y. Coudière, J.P. Vila, P. Villedieu, Convergence rate of a finite volume scheme for a two dimensional convection–diffusion problem, M2AN 33 (3) (1999) 493–516.
[48] Y. Coudière, P. Villedieu, Convergence rate of a finite volume scheme for the linear convection–diffusion equation on locally refined meshes, M2AN 34 (6) (2000) 1123–1149.
[49] E. Bertolazzi, G. Manzini, On vertex reconstructions for cell-centered finite volume approximations of 2D anisotropic diffusion problems, Math. Models Meth. Appl. Sci. 17 (1) (2007) 1–32.
[50] G. Manzini, A. Russo, A finite volume method for advection–diffusion problems in convection dominated regimes, Comput. Meth. Appl. Mech. Eng. 197 (2008) 1242–1261.
[51] Z. Sheng, G. Yuan, A nine point scheme for the approximation of diffusion operators on distorted quadrilateral meshes, SIAM J. Sci. Comput. 30 (3) (2008) 1341–1361.

[52] C. Le Potier, Schéma volumes finis monotone pour des opérateurs de diffusion fortement anisotropes sur des maillages de triangles non structurés (in french), C.R. Acad. Sci. Paris Ser. 1 341 (2005) 787–792.
[53] I.V. Kapyrin, A family of monotone methods for the numerical solution of three-dimensional diffusion problems on unstructured tetrahedral meshes, Doklady Math. 76 (2) (2007) 734–738.
[54] K. Lipnikov, M. Shashkov, D. Svyatskiy, Y. Vassilevski, Monotone finite volume schemes for diffusion equations on unstructured triangular and shape-regular polygonal meshes, J. Comput. Phys. 227 (2007) 492–512.
[55] G. Yuan, Z. Sheng, Monotone finite volume schemes for diffusion equations on polygonal meshes, J. Comput. Phys. 227 (2008) 6288–6312.
[56] G. Meurant, Computer Solutions of Large Linear Systems, Elsevier, 1999.
[57] P. Guillaume, V. Latocha, Numerical convergence of a parametrisation method for the solution of highly anisotropic two-dimensional elliptic problem, J. Scient. Comp. 25 (2005) 423–444.
[58] P.I. Crumpton, G.J. Shaw, A.F. Ware, Discretisation and multigrid solution of elliptic equations with mixed derivative terms and strongly discontinuous coefficients, J. Comput. Phys. 116 (1995) 343–358.
[59] F. Hermeline, Numerical experiments with the DDFV method, in: R. Eymard, J.M. Herard (Eds.), Finite Volumes for Complex Applications (V), Wiley, 2008, pp. 851–863.